Daily heart rate variability biofeedback training decreases locus coeruleus MRI contrast in younger adults in a randomized clinical trial

Shelby L. Bachman[a], Steve Cole[b], Hyun Joo Yoo[a], Kaoru Nashiro[a], Jungwon Min[a], Noah Mercer[a], Padideh Nasseri[a], Julian F. Thayer[c], Paul Lehrer,[d] & Mara Mather[a*]

[a]University of Southern California, Los Angeles, CA 90089

[b]University of California Los Angeles, Los Angeles, CA 90095

[c]University of California Irvine, Irvine, CA 92697

[d]Rutgers University, Piscataway, NJ 08852

8/2023 citation: Bachman, S. L., Cole, S., Yoo, H. J., Nashiro, K., Min, J., Mercer, N., Nasseri, P., Thayer, J. F., Lehrer, P., & Mather, M., (in press). Daily heart rate variability biofeedback training decreases locus coeruleus MRI contrast in younger adults in a randomized clinical trial. *International Journal of Psychophysiology*.

*Correspondence concerning this article should be addressed to: Mara Mather,

3715 McClintock Avenue, Los Angeles, CA 90089. E-mail: mara.mather@usc.edu

Abstract

As an arousal hub region in the brain, the locus coeruleus (LC) has bidirectional connections with the autonomic nervous system. Magnetic resonance imaging (MRI)-based measures of LC structural integrity have been linked to cognition and arousal, but less is known about factors that influence LC structure and function across time. Here, we tested the effects of heart rate variability (HRV) biofeedback, an intervention targeting the autonomic nervous system, on LC MRI contrast and sympathetic activity. Younger and older participants completed daily HRV biofeedback training for five weeks. Those assigned to an experimental condition performed biofeedback involving slow, paced breathing designed to increase heart rate oscillations, whereas those assigned to a control condition performed biofeedback to decrease heart rate oscillations. At the pre- and post-training timepoints, LC contrast was assessed using turbo spin echo MRI scans, and RNA sequencing was used to assess cAMP-responsive element binding protein (CREB)-regulated gene expression in circulating blood cells, an index of sympathetic nervous system signaling. We found that left LC contrast decreased in younger participants in the experimental group, and across younger participants, decreases in left LC contrast were related to the extent to which participants increased their heart rate oscillations during training. Furthermore, decreases in left LC contrast were associated with decreased expression of CREB-associated gene transcripts. On the contrary, there were no effects of biofeedback on LC contrast among older participants in the experimental group. These findings provide novel evidence that in younger adults, HRV biofeedback involving slow, paced breathing can decrease both LC contrast and sympathetic nervous system signaling.

Keywords: biofeedback, CREB, heart rate variability, locus coeruleus, norepinephrine, sympathetic nervous system

Abbreviations: CREB = cAMP-responsive element binding protein; HRV = heart rate variability; LC = locus coeruleus; MPRAGE = magnetization prepared rapid acquisition gradient echo; MRI = magnetic resonance imaging; NTS = nucleus tractus solitarii; SD = standard deviation; SNS = sympathetic nervous system; TSE = turbo spin echo

Daily heart rate variability biofeedback training decreases locus coeruleus MRI contrast in younger adults

1 Introduction

The locus coeruleus (LC), a small nucleus in the brainstem, helps coordinate the brain's arousal system. Situated at the lateral floor of the fourth ventricle, the LC serves as the brain's primary source of the neurotransmitter noradrenaline (Schwarz & Luo, 2015). Noradrenaline released from the LC to the brain and spinal cord regulates wakefulness, coordinates adaptive behavior, and modulates processes of learning and memory (Berridge & Waterhouse, 2003; Sara, 2009). Via β-adrenergic receptors, noradrenaline activates cAMP, which in turn activates cAMP-response-element-binding protein (CREB; Lorton & Bellinger, 2015; Roseboom & Klein, 1995; Thonberg et al., 2002). CREB is a stimulus-induced transcription factor that affects the expression of many different genes (Shaywitz & Greenberg, 1999). The LC is also implicated in the neuropathological progression of Alzheimer's disease, with abnormal tau evident in the LC in younger adults before cortical tau tangles emerge (Braak et al., 2011; Harley et al., 2021). LC neurodegeneration is characteristic of Alzheimer's disease (Chalermpalanupap et al., 2017), and older adults with relatively lower cell density within the LC exhibit faster rates of cognitive decline prior to death (Wilson et al., 2013).

In recent years, specialized magnetic resonance imaging (MRI) sequences have accelerated study of the human LC via their ability to quantify LC structure in vivo (Sasaki et al., 2006). In these sequences, the LC exhibits elevated MRI signal contrast relative to surrounding tissue. The properties of the LC that lead to its high MRI contrast are still under investigation (He et al., 2022; Priovoulos et al., 2020; Trujillo et al., 2017; Watanabe, 2022; Watanabe et al., 2019). MRI sequences that provide high LC contrast have been referred to as 'neuromelanin MRI' as high resolution post-mortem imaging followed by histology on the same tissue revealed that high

MRI contrast corresponded spatially with LC neurons containing neuromelanin (Keren et al., 2015; see also Cassidy et al. 2019; Kitao et al. 2013). However, there is growing evidence that neuromelanin in LC neurons is not the factor driving LC MRI contrast. In mice, LC noradrenergic neurons produced high contrast with magnetization transfer MRI, even though no neuromelanin is observed in the LC of mice (Watanabe et al., 2019). Furthermore, neuromelanin on its own does not affect magnetization transfer (Priovoulos et al., 2020; Trujillo et al., 2017) and only leads to T1 shortening at levels that are higher than neuromelanin levels in the human brain (Priovoulos et al., 2020). Instead, it seems that the property driving MRI contrast is a lower macromolecular-to-free-water fraction within the LC (Priovoulos et al., 2020; Trujillo et al., 2017; Watanabe, 2022; Watanabe et al., 2019). LC neurons tend to have large cell bodies (e.g., see the "plump" LC neuron cell bodies in Fig. 1 of Ramon-Moliner, 1974): In humans, LC neuron somas are ~37 μm in diameter (Baker et al., 1989), whereas the somas of prefrontal neurons, for comparison, are 13-17 μm in diameter (Rajkowska & Goldman-Rakic, 1995). Insofar as it is the high water content in LC cells that drives LC MRI contrast, both the number of LC cells and their current cell body size should influence LC MRI contrast.

Higher LC MRI contrast is associated with better cognitive outcomes in older adults (Dahl et al., 2019; Hämmerer et al., 2018; Liu et al., 2020), higher subjective cognition (Bell et al., 2022), reduced risk of developing mild cognitive impairment (Elman et al., 2021) or Alzheimer's disease (Galgani et al., 2023), and fewer preclinical Alzheimer's disease indicators (Jacobs et al., 2021). However, the relationship between LC contrast and brain structure varies depending on age (Bachman et al., 2021). Specifically, we found that, whereas in older adults contrast of the rostral LC was positively associated with cortical thickness in various brain regions in younger adults caudal LC contrast showed negative associations with cortical thickness (Bachman et al., 2021).

Other findings also suggest that higher LC contrast is not always a positive indicator. For instance, one study found that LC volume - also quantified using an MRI sequence that yields elevated signal intensity in the LC - was positively correlated with anxious arousal and self-reported general distress in younger adults (Morris et al., 2020). Likewise, another study found that participants with higher LC contrast had lower heart rate variability (Mather et al., 2017). In animal studies, anxiety is associated with increased tonic LC activity (Harley & Yuan, 2021; McCall et al., 2015). The higher LC MRI contrast associated with lower HRV and higher anxiety (Mather et al., 2017; Morris et al, 2020) may be driven by influences of high tonic levels of LC activity on the macromolecular-to-free-water fraction within the LC in people who have lower parasympathetic activity or higher anxiety.

Therefore, the apparently discrepant findings in younger versus older adults may be explained by different factors contributing to LC contrast throughout the lifespan. In younger individuals, the tonic level of LC activity is the primary factor influencing individual differences in LC contrast, whereas later in life, neurodegeneration becomes the dominant factor influencing individual differences in LC contrast.

Tonic LC activity and neurodegeneration could each influence LC contrast by affecting LC cellular water content, but through different means. First, in early life, current anxiety/arousal states could influence the current water content of LC cells by influencing the tonic activity level of LC neurons. Stimulating neuronal activity shrinks the volume of the interstitial fluid-filled space around neurons by approximately 30% due to uptake of water by neurons and astrocytes (Østby et al., 2009). Transport of Na+ and other ions across the cell membrane during neuronal activity triggers water movement across the cell membrane against the osmotic gradient (MacAulay, 2021). In the cortex, researchers have observed that a β-adrenergic agonist decreases interstitial volume (Sherpa et al., 2016), while adrenergic antagonists increase interstitial volume

(Xie et al., 2013). Thus, both general neuronal activity and specifically noradrenergic activity may influence the relative fluid volume of brain cells and the spaces around them, which could influence the magnetization transfer signal from the LC, although to date we lack studies tracking activity-based changes in cell size in the locus coeruleus. In later life, individual differences in neurodegeneration of LC neurons that affect free water concentrations (e.g., Chu et al., 2021) may account for a greater share of variance in individual differences in LC contrast than activity-related fluctuations in cell body volume.

Despite what has been learned about the LC from recent MRI studies, no published studies have assessed whether there are interventions that can change LC MRI contrast. What type of interventions might change LC contrast over time? Because the LC is a key player in the stress response and has bidirectional connections with the parasympathetic and sympathetic branches of the autonomic nervous system (Wood et al., 2017), we reasoned that an intervention targeting the autonomic nervous system could influence LC structure. One such intervention is heart rate variability (HRV) biofeedback (Lehrer & Gevirtz, 2014). Individuals with higher HRV, an index of parasympathetic control over heart rate and autonomic regulation (Mulcahy et al., 2019; Thayer & Lane, 2000), are better able to regulate their emotions and exhibit reduced physiological responses to stressors (Thayer & Lane, 2009; Weber et al., 2010), relative to those with lower HRV. HRV can be systematically manipulated through biofeedback that involves slow, paced breathing and simultaneous feedback on the coupling between heart rate oscillations and breathing (Lehrer & Gevirtz, 2014). Slow breathing, particularly at a pace around 10 seconds per breath, elicits high-amplitude oscillations in heart rate (Lehrer et al., 2003). Slow breathing also stimulates the vagus nerve (Brown & Gerbarg, 2005), which sends projections to the LC by way of the nucleus tractus solitarii (NTS; Badran et al., 2018; Fornai et al., 2011). Performing HRV biofeedback over a period of weeks has been shown to reduce levels of stress and anxiety

(Goessl et al., 2017) in younger as well as older adults (Jester et al., 2019), but it is unknown whether HRV-biofeedback affects the LC's structure and function.

Here, we examined whether HRV biofeedback affected LC MRI contrast and sympathetic activity. Younger and older participants completed 5 weeks of HRV biofeedback training as part of a clinical trial testing the effects of HRV biofeedback training on brain regions involved in emotion regulation (Clinicaltrials.gov NCT03458910 "Heart Rate Variability and Emotion Regulation," Nashiro et al., 2023; Yoo et al., 2023). Participants randomized to an experimental condition completed daily biofeedback involving slow, paced breathing to increase heart rate oscillations and HRV, whereas participants randomized to an active control condition completed daily biofeedback training designed to decrease heart rate oscillations and HRV. We designed this novel active control condition in order to equate as many features of the intervention as possible while maximizing differences in heart rate oscillations. As an exploratory outcome, both before and after the 5-week training period, we assessed LC contrast in all participants using turbo spin echo (TSE) MRI scans that exhibit elevated signal intensity in the LC. Based on prior work demonstrating beneficial effects of HRV on emotional well-being, and in line with our hypotheses regarding LC contrast reflecting stress in younger adults, we expected that performing 5 weeks of HRV biofeedback training would decrease LC contrast in younger participants. Conversely, as we hypothesize that neurodegeneration, more so than tonic LC activity levels, contributes to variance in LC contrast in older adulthood, we predicted that HRV biofeedback would not decrease LC contrast in older participants. Furthermore, in a subset of younger participants, we collected blood samples before and after the training period to assess changes in a health-relevant index of sympathetic nervous system (SNS) activity – blood cell expression of genes regulated by the cAMP-responsive element binding protein (CREB) family of transcription factors, which mediates beta-adrenergic signaling from the SNS (Cole et al., 2010; Mayr &

Montminy, 2001). In this subset, we predicted that training-related decreases in LC contrast would be coupled with decreases in SNS signaling and thereby reduce expression of CREB-regulated gene transcripts. Previous research has validated blood cell CREB-associated RNA expression levels as a measure of β-adrenergic signaling (Brown et al., 2010; Cole et al., 2005; Powell et al., 2013).

2 Materials and Methods

2.1 Participants

Data were collected as part of an intervention study testing the effects of 5 weeks of HRV biofeedback training in younger and older adults (ClinicalTrials.gov NCT03458910; for a full description of the study, see Yoo et al., 2023). Eligible participants were healthy, MRI-eligible younger adults between the ages of 18 and 35 and older adults between the ages of 55 to 80 (for more details including determination of sample size see Yoo et al, 2023). Potential participants were recruited via the USC Healthy Minds community subject pool, a USC online bulletin board, Facebook, and flyers between February 2018 and March 2020 (enrollment was cut short by the COVID pandemic). Individuals who regularly practiced biofeedback training or breathing techniques were excluded from participation. Older adults were screened for cognitive dysfunction by telephone using the TELE interview (Gatz et al., 1995); individuals scoring below 16 were excluded from participation.

2.2 Study Procedures Overview

Participants were scheduled in waves in small groups (each group meeting weekly in our lab on the USC campus on a different day of the week). After scheduling for a wave was complete, each group was randomized to one of the two conditions (for more information, see Yoo et al., 2023). Participants were blinded to researcher hypotheses regarding differential

outcomes by condition. Those in an increase-oscillations (Osc+) condition completed 20-40 minutes of daily biofeedback training involving slow, paced breathing which was designed to increase heart rate oscillations and HRV. Participants in a decrease-oscillations (Osc-) condition completed 20-40 minutes of biofeedback training per day designed to decrease heart rate oscillations and HRV.

As part of the intervention study which lasted 7 weeks, MRI assessments were conducted at a pre-training timepoint (second study week), before participants learned about or practiced the intervention, and following 5 weeks of biofeedback training (seventh study week). A total of 175 participants (115 younger, 60 older) completed pre- and/or post-training MRI assessments, yielding a total of 325 TSE scans (detailed breakdown in the Supplementary Methods, Section 1). A flow chart detailing enrollment and dropouts is provided in Yoo et al., (2023, Fig. 1). Following exclusions for artifact or motion on native TSE scans (Section 2.3.1), 287 scans were used for LC delineation. Additional exclusions were applied due to artifact after warping TSE scans to MNI152 space (Section 2.3.1). In addition, blood samples were collected from a subset of 54 younger participants at pre- and post-training timepoints (first and sixth study weeks, respectively) to assess change in expression of genes regulated by CREB. A total of 129 participants (93 younger, 36 older) with LC contrast values and/or blood-based measures available at both timepoints were included for analysis. Characteristics of this sample are presented in Table 1. The University of Southern California Institutional Review Board approved the study. All participants provided written, informed consent prior to participation and received monetary compensation for their participation.

Table 1. *Sample characteristics.*

Age group	Condition	N	N (%) Female	Age, mean (SD)	Age, range	Education, mean (SD)	Education, range
Younger	Osc+	47	26 (55.3%)	22.64 (2.57)	18-28	15.99 (1.87)	12-20
Younger	Osc-	46	24 (52.2%)	22.57 (3.24)	18-31	15.74 (2.64)	12-24
Older	Osc+	17	12 (70.6%)	65 (6.86)	55-80	17.12 (2.71)	14-25
Older	Osc-	19	15 (78.9%)	65.21 (5.61)	57-77	16.53 (2.39)	14-22

Note. Age and education are expressed in years. Osc+ = increase-oscillations condition; Osc- = decrease-oscillations condition; SD = standard deviation.

2.3 Heart Rate Biofeedback and Pulse Measurement

During the home training sessions, participants received biofeedback, seeing a continuously updating line indicating heart rate over time. Osc+ participants tried to make their heart rate oscillate, tracking their breathing, and Osc- participants tried to keep their heart rate steady. Heart rate was measured using an infrared pulse plethysmograph sensor clipped to the participant's earlobe and attached via USB to a small laptop running emWave Pro (HeartMath®Institute, 2020) software (for more details see Nashiro et al., 2023). As already reported, we computed autoregressive spectral power for each training session (Yoo et al., 2022). For each participant, we averaged the spectral power across all home training sessions and extracted the summed power within the 0.063– 0.125 Hz (8-16s) range to provide a measure of training oscillatory power in a frequency range encompassing the breathing rates used by the Osc+ participants. The resulting value of training oscillatory power reflected how much each participant increased their heart rate oscillations on average during biofeedback training. Training oscillatory power values were log transformed prior to statistical analysis. A total of 2 Osc- participants included in analyses of LC contrast change were missing values of training oscillatory power.

2.4 MRI data collection

MRI data were collected at the University of Southern California David and Dana Dornsife Neuroimaging Center, on a Siemens Magnetom Trio 3T MRI scanner with a 32-channel head coil. Sequences relevant to the present analyses are described below.

A high-resolution, T_1-weighted magnetization prepared rapid acquisition gradient echo (MPRAGE) scan was acquired (TR = 2300ms, TE = 2.26 ms, flip angle = 9°, bandwidth = 200 Hz/Px, isometric voxel size = 1.0mm^3, no gap between slices, 175 volumes). Based on the MPRAGE scan, a two-dimensional, multi-slice TSE scan was collected by aligning the field of view perpendicular to the respective participant's brainstem. Parameters of this TSE sequence were as follows: TR = 750ms, TE = 12ms, flip angle = 120°, bandwidth = 287 Hz/Px, voxel size = 0.43 x 0.43 x 2.5mm, gap between slices = 1mm. The TSE sequence included 11 axial slices and covered the entire pons. TSE scans from randomly selected participants are shown in Figure 1A.

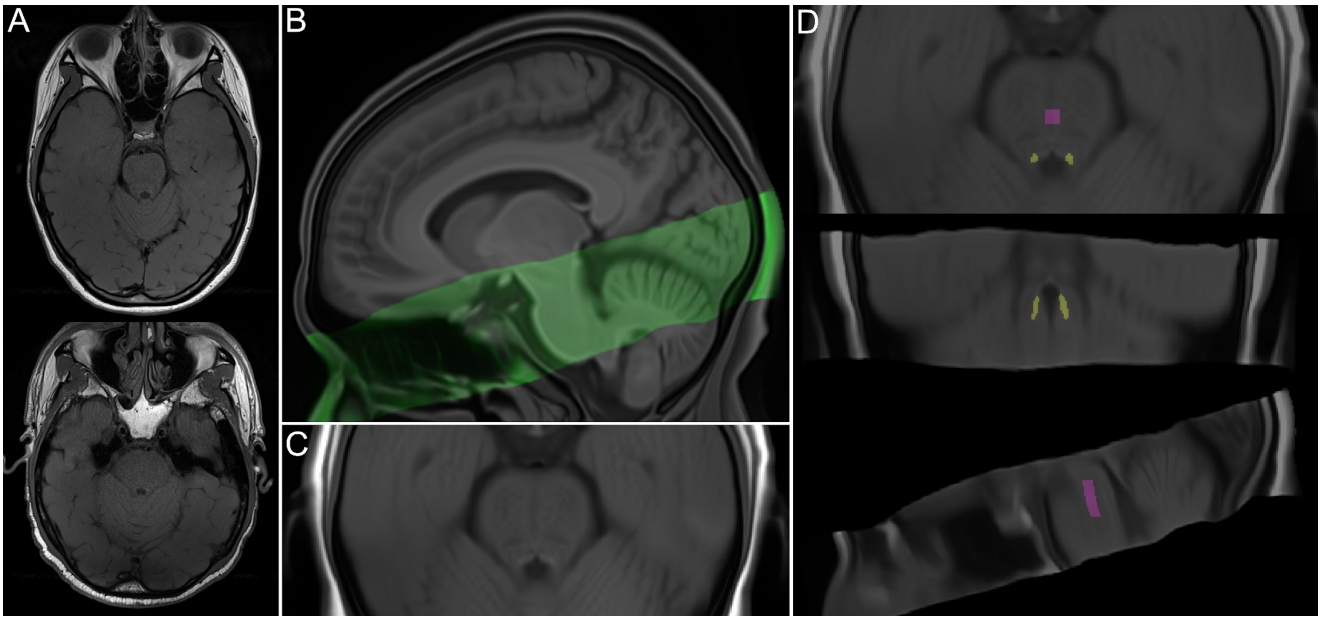

Figure 1. (A) Turbo spin echo (TSE) scans from randomly selected younger (top) and older (bottom) participants. (B) Sagittal view of TSE template (green) overlaid onto whole-brain template, both warped to MNI152 0.5mm (linear) space. (C) Detailed axial view of TSE template, warped to MNI152 space. (D) TSE template, warped to MNI152 space, overlaid with locus coeruleus meta-mask and pontine reference region from Dahl et al. (2022), which were used for calculation of LC contrast ratios.

2.5 MRI data analysis

2.5.1 LC delineation.

We used a semi-automated method to delineate the LC on all available pre- and post-training TSE scans based on approaches described by Dahl et al. (2019) and Ye et al. (2021). LC delineation steps were performed using Advanced Normalization Tools (ANTs; Version 2.3.4; Avants et al., 2011; http://stnava.github.io/ANTs/). Visualization steps were performed using ITK-SNAP (Version 3.8.0; Yushkevich et al., 2006; http://www.itksnap.org). Parameters for each step are described in the Supplementary Methods (Section 2).

All TSE scans were first visually inspected; scans with excessive motion or susceptibility artifact overlapping the LC or pons (n = 34), incorrect positioning (n = 3), or different resolution (n = 1) were excluded from LC delineation (Supplementary Methods, Section 1). The remaining TSE and corresponding MPRAGE scans were upsampled to twice their native resolution using the ResampleImage ANTs routine. Upsampled MPRAGE scans were used to generate a whole-brain template with the antsMultivariateTemplateConstruction.sh routine (Figure 1B; see Supplementary Methods Section 2 for a description of template-building procedures). Each TSE scan was then coregistered to its corresponding whole-brain template-coregistered MPRAGE scan, using the antsRegistrationSyNQuick.sh routine. All coregistered TSE scans were used to build a TSE template (Figures 1B and 1C). Using the antsRegistrationSyN.sh routine, the resulting TSE template was coregistered to the whole-brain template to ensure spatial alignment. The whole-brain template was then coregistered to MNI152 0.5mm (linear) standard space, in order to facilitate comparison with previously-published LC maps. Transforms from all template-building and coregistration steps described above were applied in a single step to warp upsampled TSE scans to MNI152 space, using the antsApplyTransforms.sh routine. In addition, transforms from the final coregistration steps were applied to warp the TSE template to MNI152 space (Figure 1C). As a validation step, we examined whether locations of hyperintensity on the TSE template in MNI152 space aligned with the location of the Dahl et al. (2022) meta-map, which was generated by aggregating across published LC maps and thus reflected a plausible LC volume of interest with high agreement across studies. (For discussion of a template-space approach to LC localization, see Giorgi et al., 2022.) We found high correspondence between hyperintensities on the TSE template and the LC meta-map (Supplementary Figure S1).

At this stage, a total of 6 warped TSE scans were excluded from LC delineation after visually confirming that, once warped to MNI152 space, they contained artifacts overlapping the

LC or central pons. This left data from 78 younger (39 Osc+, 39 Osc-) and 36 older (17 Osc+, 19 Osc-) participants included for LC delineation and analyses of change in LC contrast[1]. We proceeded to delineate the LC for individual participants and timepoints by applying the Dahl et al. (2022) LC meta-map as a mask on all warped TSE scans (Figure 1D). Within the masked region of each scan, we extracted the intensity and location of the peak-intensity LC voxel in each *z*-slice and hemisphere. As another validation step, we compared the resulting intensity values to intensity values determined through manual delineation of the LC on native-resolution TSE scans (Supplementary Methods, Section 3). Two-way mixed-effects intraclass correlation analyses based on consistency indicated high correspondence between peak LC intensity values from the semi-automated and manual methods for the left LC ($ICC(3, 1) = 0.939$, *95% CI* = 0.921 - 0.953, $p < .001$) and right LC ($ICC(3, 1) = 0.924$, *95% CI* = 0.902 - 0.941, $p < .001$). To compute LC contrast ratios reflecting peak LC intensity relative to that of surrounding tissue, we also extracted intensity values from a central pontine region (Figure 1D). Specifically, we applied the central pontine reference map from Dahl et al. (2022) as a mask on individual TSE scans that had been warped to MNI space and extracted the peak intensity value within the masked region.

2.5.2 Calculation of LC MRI contrast.

LC MRI contrast is typically calculated as a ratio reflecting peak signal intensity in the LC relative to peak intensity within a pontine reference region (Liu et al., 2017):

$$LC\ contrast = \frac{intensity(LC) - intensity(pons)}{intensity(pons)}$$

[1] Welch's *t*-tests indicated that participants who were included versus excluded from analysis did not differ significantly in terms of age, $t(57.0) = 0.23$, $p = .817$, or education level, $t(64.8) = 0.57$, $p = .571$. A Chi-squared test of independence indicated that the distribution of females versus males differed when comparing participants who were included versus excluded for the purpose of analysis, $\chi^2(3) = 86.85$, $p < .001$; in particular, 58.1% of participants included for analysis were females, 43.6% of participants excluded from analysis were females.

No published studies have examined the stability of peak LC signal intensity locations across time, or factors which influence locations of peak LC intensity, thus we performed an exploratory step to guide our calculation of LC contrast. Specifically, we assessed whether, for each participant, locations of peak intensity in each left and right LC shifted from pre- to post-training (peak LC intensity locations are depicted in Supplementary Figure S2A). To do so, we calculated for each participant the 3-dimensional distance between peak LC intensity locations at the pre- and post-training timepoints, for left and right LC separately (Supplementary Figure S2B). A linear mixed effects analysis indicated that these distances differed from 0 across training conditions, age groups and hemispheres ($p <$. 001; Supplementary Results, Section 1), suggesting that locations of peak LC intensity were not consistent within individuals across time. This is not surprising in that the LC voxel with peak intensity is not necessarily an outlier and there may be other voxels with similar intensity values. In this type of situation, random noise may lead to different high contrast voxels to be identified as the peak voxel in different scan sessions. We therefore aimed to calculate LC contrast in a way that was not biased by peak LC signal intensity location at either the pre- or post-training timepoint. Specifically, for each participant, we calculated LC contrast at each timepoint as an average of LC contrast at the locations of pre- and post-training peak LC signal intensity.

In addition to calculating LC contrast based on locations of peak LC intensity, we calculated values of rostral and caudal LC contrast. For this step, we used the locations of rostral and caudal clusters along the LC's rostrocaudal axis where we previously found age differences in LC contrast (Dahl et al., 2019; rostral: MNI z = 101-104; caudal: MNI z = 87-95). For each participant and timepoint, contrast ratios in each z-slice and hemisphere were calculated, then ratios were averaged across hemispheres for each z-slice. Finally, ratios were averaged across the

caudal and rostral clusters of slices to obtain a value of rostral and caudal LC contrast, respectively, for each participant.

2.6 Blood sampling and RNA sequencing analysis

For a subset of participants (N = 54 younger adults: 30 Osc+, 24 Osc-), peripheral blood samples were collected under resting conditions at the pre- and post-training timepoints by antecubital venipuncture into PAXgene RNA tubes. Following collection, samples were gently inverted ten times and kept at room temperature for between 2.00 and 70.20 hours (mean = 6.95 hours). Samples were then stored frozen at -80°C at the USC School of Gerontology before they were transferred and assayed in a single batch at the UCLA Social Genomics Core Laboratory, as previously described (Cole et al., 2020). Briefly, total RNA was extracted from 2.5 ml blood samples using an automated nucleic acid processing system (QIAcube; Qiagen), checked for suitable RNA integrity and mass (>50 ng by NanoDrop One spectrophotometry; achieved mean = 4497 ng) and assayed by RNA sequencing in the UCLA Neuroscience Genomics Core Laboratory using Lexogen QuantSeq 3' FWD cDNA library synthesis and multiplex DNA sequencing on an Illumina HiSeq 4000 instrument with single-strand 65-nt sequence reads (all following the manufacturer's standard protocol). Analyses targeted >10 million sequence reads per sample (achieved mean 15.1 million), each of which was mapped to the RefSeq human transcriptome sequence using the STAR aligner (achieved average 94% mapping rate) to generate transcript counts per million total transcripts (TPM). TPM values were floored at 1 TPM to reduce spurious variability, log2-transformed to reduce heteroscedasticity, and analyzed by linear statistical models with promoter sequence-based bioinformatics analyses of CREB activity as described below.

2.7 Statistical analysis

We fit a linear mixed effects model to assess the fixed effects of timepoint, training condition, age group and hemisphere on LC contrast. Mixed models were also fit for each age group separately to examine the fixed effects of timepoint, training condition, hemisphere and their interactions on LC contrast. Significant timepoint x condition interactions were supplemented with post hoc comparisons of pre- versus post-training LC contrast for each training condition and hemisphere.

Next, we tested whether changes in LC contrast were related to the extent to which participants increased their heart rate oscillations during biofeedback training. For each participant, values of change in left and right LC contrast were calculated as the difference between pre- and post-training LC contrast values. We then fit another mixed model testing the fixed effects of training oscillatory power (see Section 2.3 for details of this measure), hemisphere, age group, and their interactions on LC contrast. For each age group and hemisphere separately, we also performed planned Pearson correlation analyses to test associations between change in LC contrast and training oscillatory power. Supplementary analyses were performed to assess training effects on rostral and caudal LC contrast (Supplementary Methods, Section 4).

Based on previous findings of sex differences in LC contrast (Bachman et al., 2021; but see Betts et al., 2017, Liu et al., 2019, Trujillo et al., 2019, and Ye et al., 2022), sex differences in the responsiveness of the LC to stress (Bangasser et al., 2016), sex differences in potentially LC-related cognitive strategies (Ycaza Herrera et al., 2019), and sensitivity of the LC to sex hormones (Bangasser et al., 2016; Luckey et al., 2021), we tested for sex differences in LC contrast change and its relationship with training oscillatory power by fitting the previously described mixed models including sex and its interactions as fixed effects (Supplementary Methods, Section 5). These analyses were performed only for younger participants (Osc+: 24

female, 15 male; Osc-: 18 female, 21 male) because we were underpowered to detect sex differences among older participants.

These analyses were performed in R (Version 4.1.0; R Core Team, 2021). Linear mixed effects models were fit using the R package `lme4` (Version 1.1-27.1; Bates et al., 2015), and significance of fixed effects was assessed with Satterthwaite's method as implemented in the R package `lmerTest` (Version 3.1-3; Kuznetsova et al., 2017). All models included random intercepts for participants. A sum coding contrast scheme was applied to factor variables (condition: Osc+ = 0.5, Osc- = 0.5; timepoint: post-training = 0.5, pre-training = 0.5; age group: older = 0.5, younger = -0.5; hemisphere: left = 0.5, right = -0.5; sex: female = 0.5, male = -0.5). Post hoc comparisons of model-estimated marginal means were performed with a Bonferroni correction for multiple comparisons, as implemented in the `emmeans` R package (Version 1.6.2-1; Lenth, 2021). Effect sizes were calculated using the R package `effectsize` (Version 0.5; Ben-Shachar et al., 2020) and reported as *d*.

We also tested whether training condition (Osc+ or Osc-) or change in LC contrast was associated with change in CREB activity from pre- to post-training using an established bioinformatic measure of CREB gene regulation employed in previous research (Cole et al., 2020). Data from 54 younger participants (30 Osc+, 24 Osc-) with available blood-based measures at both timepoints were included for analysis of CREB activity change by training condition, and data from 39 younger participants (22 Osc+, 17 Osc-) with available blood-based measures and LC contrast values at both timepoints were included for analysis of associations between CREB activity change and LC contrast change. In these analyses, whole transcriptome profiling data were screened to identify genes that showed > 1.5-fold differential change over time between conditions or > 1.5-fold differential change in expression per standard deviation (SD) of pre- to post-training LC contrast change, and the core promoter DNA sequences of those

genes were scanned for the prevalence of CREB-binding motifs using the TELiS database (Cole et al., 2020; Cole et al., 2005). Analyses were conducted as previously described (Cole et al., 2020), with CREB activity quantified by the ratio of CREB-binding site prevalence (defined by TRANSFAC position-specific weight matrix V$CREB_Q4) in genes up-regulated in association with condition differences in change or LC contrast change (i.e., >1.5-fold upregulation from pre- to post-training timepoint per SD of LC contrast change) vs. down-regulated (>1.5-fold down-regulated), and log2-ratios averaged over 9 parametric combinations of promoter sequence length (-300, -600, and -1000 to +200 bp relative to the RefSeq transcription start site) and detection stringency (TRANSFAC mat_sim = .80, .90, and .95). Statistical significance was assessed using standard errors derived from bootstrap resampling of linear model residual vectors in underlying gene expression data, which controls for correlation across genes. For additional details on analytic methods, see Cole et al. (2005) and Cole et al. (2020).

3 Results

3.1 LC contrast decreased in younger participants in the Osc+ condition

LC contrast at the pre- and post-training timepoints is shown in Figure 2A. Using independent samples t-tests, we first confirmed that there were no significant baseline differences in the LC contrast among either younger, $t(76) = 1.73$, $p = .09$, $d = 0.39$ (left) and $t(76) = 0.19$, $p = .85$, $d = 0.04$ (right), or older adults, $t(34) = .46$, $p = .65$, $d = 0.15$ (left) and $t(34) = 0.003$, $p = .997$, $d = 0.001$ (right). Then, using a linear mixed effects analysis testing the fixed effects of condition, timepoint and hemisphere on LC contrast in younger participants (Table 2A), we found a significant training condition x timepoint interaction on LC contrast ($p = .034$, $d = -0.283$). Post hoc comparisons of estimated marginal means indicated that at the post- relative to the pre-training timepoint, LC contrast was numerically lower among younger participants in the Osc+ condition, left: $t(228) = -2.193$, $p = .029$, $d = -0.497$; right: $t(228) = -0.059$, $p = .953$, $d = -$

0.013 and numerically higher among younger participants in the Osc- condition, left: $t(228) = 0.599$, $p = .550$, $d = 0.136$; right: $t(228) = 1.423$, $p = .156$, $d = 0.322$. For younger participants, we also found a significant fixed effect of hemisphere on LC contrast ($p < .001$, $d = 1.462$), with left LC contrast being higher than right LC contrast, but no other fixed effects were significant. For older participants (Table 2B), we did not find a significant training condition x timepoint interaction ($p = .713$, $d = 0.073$), but we did observe a significant fixed effect of timepoint ($p = .046$, $d = 0.400$), with LC contrast being higher at the post- compared to the pre-training timepoint. As in the younger sample, we observed a significant effect of hemisphere on LC contrast in older participants ($p < .001$, $d = 1.261$), driven by higher contrast for the left relative to the right LC. Notably, in a model including data from both age groups, we did not observe significant timepoint x condition, age x timepoint x condition, or age x timepoint interactions on LC contrast (p's > .05; Supplementary Results, Section 2).

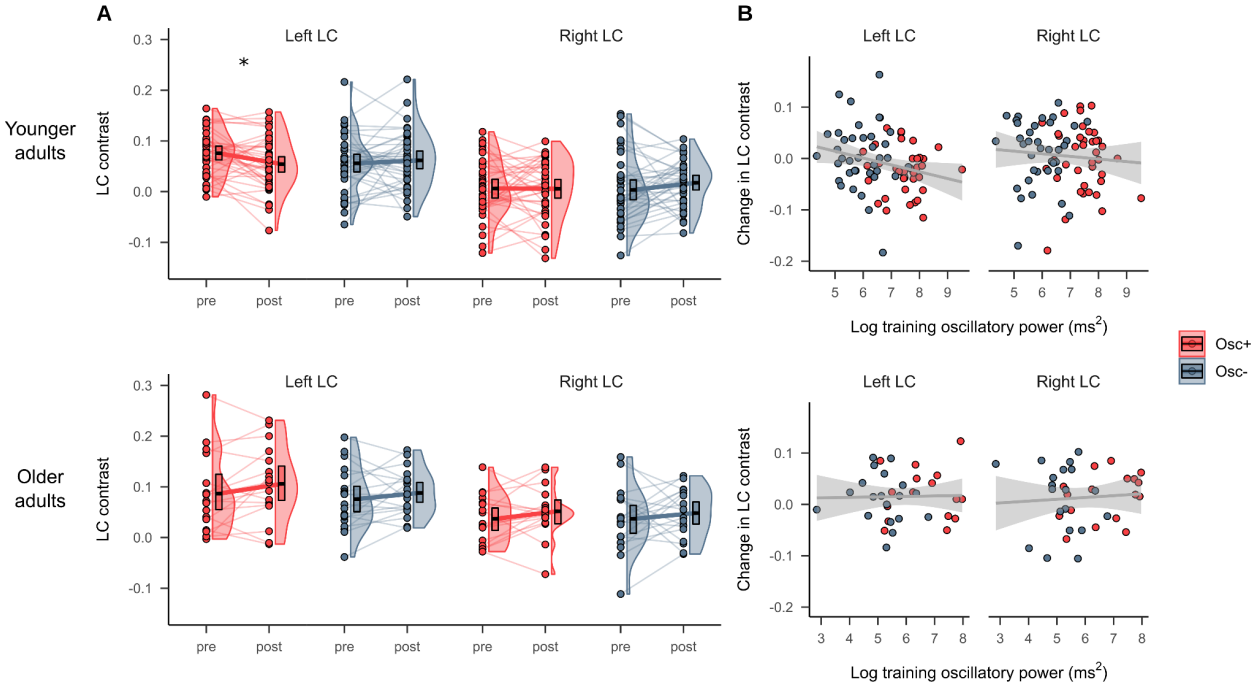

Figure 2. (A) LC MRI contrast at the pre- and post-training timepoints for the Osc+ and Osc- conditions, for younger (top) and older (bottom) participants. (B) Associations between pre- to

post-training change in LC contrast and training oscillatory power, a measure of how much participants increased their heart rate oscillations across practice sessions, for younger (top) and older (bottom) participants. Linear regression lines with 95% confidence intervals are shown in gray. Significance labels (*$p < .05$) refer to pairwise comparisons between pre- and post-training LC contrast.

Table 2:

Results of linear mixed effects analysis testing the fixed effects of timepoint, training condition, and hemisphere on LC MRI contrast, in younger adults (A) and older adults (B).

Predictor	Estimate	SE	95% CI	t	p
A. Younger adults					
Intercept	0.035	0.005	0.026, 0.044	7.657	**<.001**
Timepoint	-0.001	0.005	-0.01, 0.009	-0.115	0.909
Condition	0.001	0.009	-0.017, 0.019	0.085	0.932
Hemisphere	0.054	0.005	0.044, 0.063	11.036	**<.001**
Timepoint x Condition	-0.021	0.010	-0.04, -0.002	-2.137	**0.034**
Timepoint x Hemisphere	-0.014	0.010	-0.033, 0.005	-1.480	0.140
Condition x Hemisphere	0.011	0.010	-0.008, 0.03	1.106	0.270
Timepoint x Condition x Hemisphere	-0.013	0.019	-0.051, 0.025	-0.655	0.513
B. Older adults					
Intercept	0.066	0.008	0.051, 0.081	8.630	**<.001**
Timepoint	0.014	0.007	0, 0.029	2.021	**0.046**
Condition	0.008	0.015	-0.022, 0.038	0.515	0.610
Hemisphere	0.046	0.007	0.032, 0.06	6.366	**<.001**

Predictor	Estimate	SE	95% CI	t	p
Timepoint x Condition	0.005	0.014	-0.023, 0.033	0.368	0.713
Timepoint x Hemisphere	0.002	0.014	-0.026, 0.031	0.170	0.865
Condition x Hemisphere	0.012	0.014	-0.016, 0.041	0.867	0.388
Timepoint x Condition x Hemisphere	0.004	0.029	-0.053, 0.06	0.122	0.903

Note. Models included random intercepts for participants. Factors were coded as: timepoint (post-training = 0.5, pre-training = -0.5), condition (Osc+ = 0.5, Osc- = -0.5), hemisphere (left = 0.5, right = -0.5).

Supplementary analyses indicated no significant training condition x timepoint or training condition x timepoint x age group interaction effects on caudal LC contrast (p's >= .421). For rostral LC contrast, there was a significant training condition x timepoint x age group interaction effect (p = .044) but no significant training condition x timepoint interaction effect (p = 0.764). This 3-way interaction effect was driven by decreases in rostral LC contrast for younger participants in the Osc+ condition and increases for younger participants in the Osc- condition, and the opposite pattern in older participants, but no pairwise comparisons of rostral LC contrast were significant. These results are fully described in the Supplementary Results (Section 3).

3.2 Training oscillatory power was associated with decreases in left LC contrast

Associations between training oscillatory power and change in LC contrast are depicted in Figure 2B. In younger participants, we found a significant negative correlation between training oscillatory power and change in left LC contrast, $r(74) = -0.249$, *95% CI* = -0.449 - -0.025, p = .030, but no significant correlation between training oscillatory power and change in right LC contrast, $r(74) = -0.085$, *95% CI* = -0.305 - 0.143, p = .463. In older participants, training power was not correlated with change in either left LC contrast, $r(34) = 0.024$, *95% CI* = -0.307 - 0.35, p = .889, or right LC contrast, $r(34) = 0.076$, *95% CI* = -0.259 - 0.395, p = .660. We note that the negative association between training power and left LC contrast change in younger adults did

not emerge in a linear mixed effects analysis testing the fixed effects of training power, age group, hemisphere and their interactions on LC contrast; specifically, this analysis indicated no significant fixed effects of training power or interaction effects involving training power (p's > .05; Supplementary Results, Section 4). There were no significant correlations between change in either rostral or caudal LC contrast and training oscillatory power, in either younger or older adults (p's >= .363; Supplementary Results, Section 4).

3.3 The association between training oscillatory power and change in left LC contrast was more negative in males

Pre- and post-training LC contrast for younger males and females is shown in Figure 3A. A linear mixed effects analysis testing fixed effects of timepoint, condition, hemisphere, sex and their interactions in younger adults indicated no significant timepoint x condition x sex or timepoint x condition x hemisphere x sex interactions on LC contrast (p's > 0.05; Supplementary Results, Section 5). We note that this analysis indicated a significant fixed effect of sex on LC contrast (p = .007, d = 0.650), driven by greater LC contrast for females than males, as well as a significant timepoint x condition interaction on LC contrast (p = .032, d = -0.290), in line with what we observed above (Section 3.1). When we next added sex as a fixed effect to the model testing the effects of training oscillatory power and hemisphere on change in LC contrast (Table 3), we found a marginally significant interaction between training power and sex (p = .050, d = 0.470). This was driven by younger males having a more negative association between training power and change in LC contrast than younger females (Figure 3B). Notably, this analysis also indicated a significant fixed effect of sex (p = .048, d = -0.473), with females exhibiting greater decreases in LC contrast relative to males, and a significant fixed effect of training oscillatory power on change in LC contrast (p = .036, d= -0.505), after accounting for the effects of sex and hemisphere.

Table 3:

Results of linear mixed effects analysis testing the fixed effects of training oscillatory power, hemisphere, and sex on change in LC MRI contrast in younger adults.

Predictor	Estimate	SE	95% CI	t	p
Intercept	0.080	0.039	0.004, 0.156	2.050	**0.044**
Training power	-0.012	0.006	-0.024, -0.001	-2.142	**0.036**
Hemisphere	0.041	0.049	-0.055, 0.137	0.838	0.405
Sex	-0.157	0.078	-0.309, -0.004	-2.008	**0.048**
Training power x Hemisphere	-0.008	0.007	-0.022, 0.006	-1.132	0.261
Training power x Sex	0.023	0.012	0, 0.046	1.993	**0.050**
Hemisphere x Sex	-0.027	0.098	-0.218, 0.165	-0.273	0.785
Training power x Hemisphere x Sex	0.003	0.015	-0.025, 0.032	0.215	0.830

Note. Models included random intercepts for participants. Factors were coded as: hemisphere (left = 0.5, right = -0.5), sex (female = 0.5, male = -0.5).

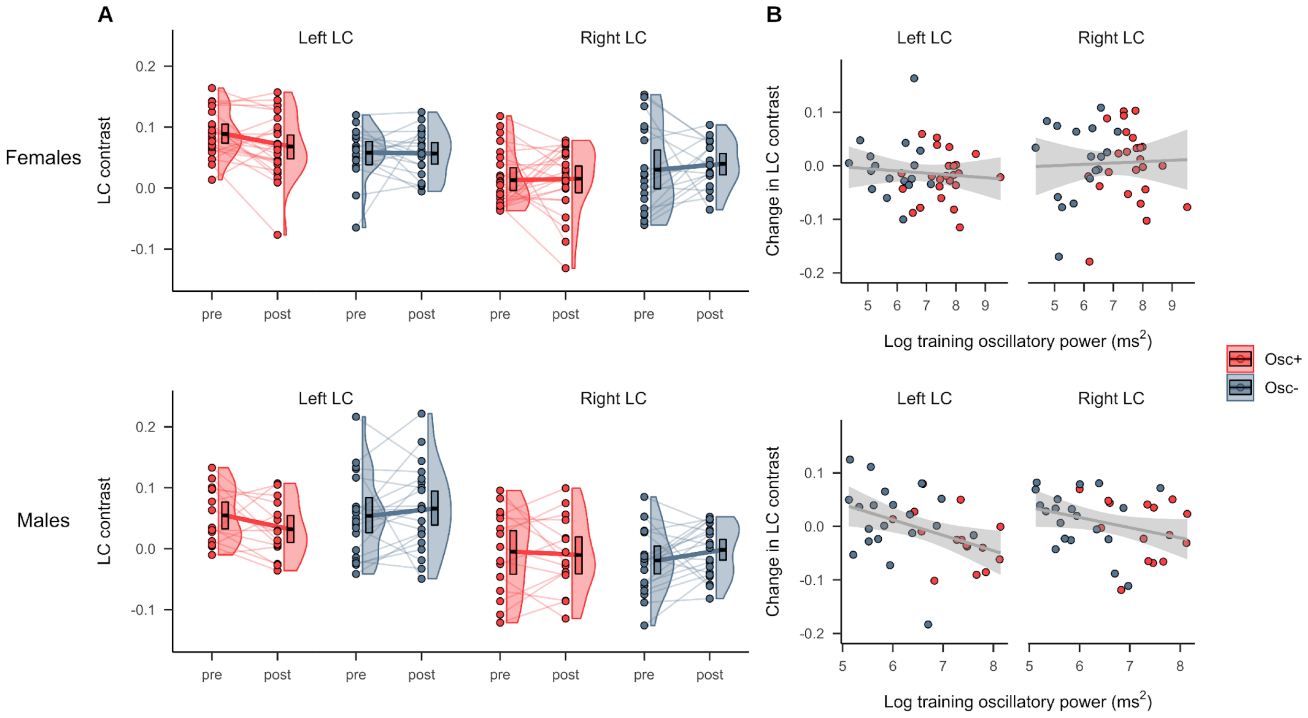

Figure 3. (A) LC MRI contrast at the pre- and post-training timepoints for younger participants in the Osc+ and Osc- conditions, stratified by sex (top = females, bottom = males). (B) Associations between change in LC contrast and training oscillatory power among younger participants, stratified by sex (top = females, bottom = males). Linear regression lines with 95% confidence intervals are shown in gray.

3.4 Decreases in left LC contrast were associated with decreases in CREB activity

Results of RNA sequencing in younger participants with available blood-based measures indicated a significant interaction between timepoint and condition on expression of genes regulated by the SNS-responsive CREB transcription factor (*bootstrap* z = -3.30, p = .001). Younger participants in the Osc- condition showed what appears to be a secular trend, with increased CREB activity from pre- to post-training (z = 2.70, p = .008), whereas participants in the Osc+ condition were buffered against that trend, showing no significant change over time (z = -0.45, p = .650).

We also found that greater change in LC contrast was associated with greater change in CREB activity (Figure 4), selectively for left LC contrast ($z = 1.97$, $p = .049$), with no significant effect for right LC contrast ($z = 0.63$, $p = .530$). In other words, participants with larger decreases in left LC contrast had larger decreases in CREB activity.

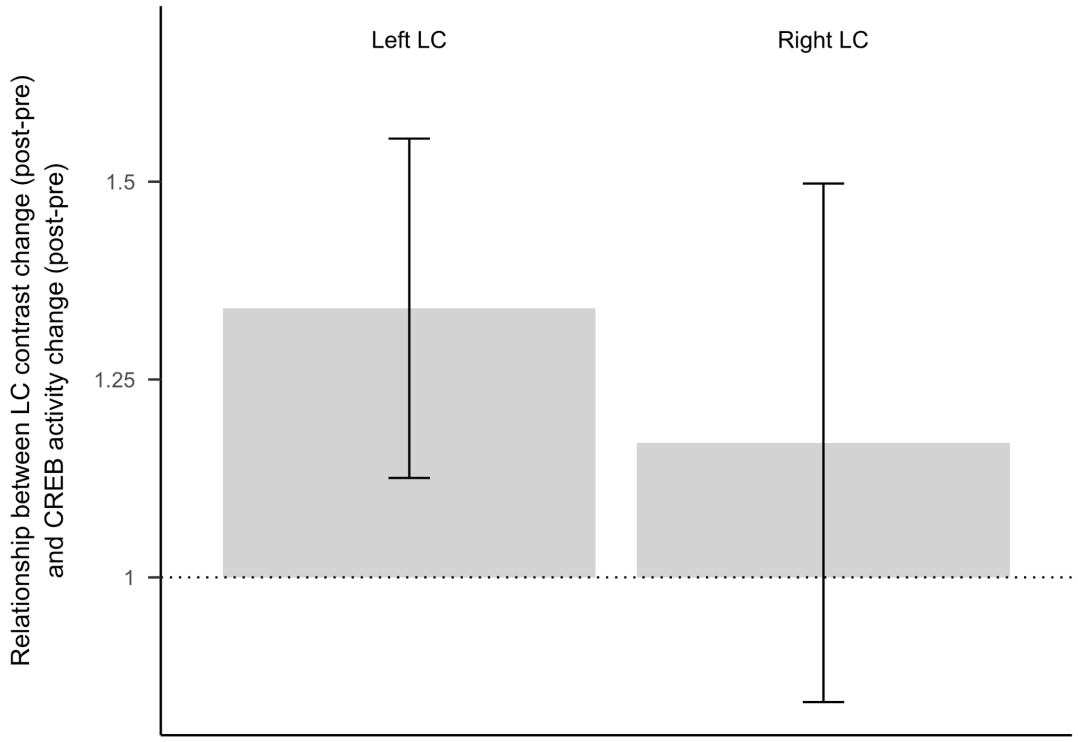

Figure 4. Regression coefficients reflecting the association between LC contrast change (post-training - pre-training) and CREB activity change (post-training - pre-training), for left and right LC separately). Error bars reflect regression coefficient standard errors derived from bootstrap resampling of linear model residual vectors in underlying gene expression data. Figure reflects data from a subset of 39 younger participants for whom both blood-based measures and LC contrast values were available (22 Osc+, 17 Osc-) .

4 Discussion

In recent years, much has been learned about how LC MRI contrast, a proxy for LC structural integrity, relates to cognition across the lifespan (Betts et al., 2019; Dahl et al., 2019;

Elman et al., 2021; Liu et al., 2020). However, no published studies have examined factors that influence LC contrast across time. Here, we found that in younger adults, performing 5 weeks of HRV biofeedback training decreased LC contrast. This effect was larger for the left LC and scaled with the extent to which participants increased their heart rate oscillations during training. We also found that among younger participants with available blood-based measures, decreases in left LC contrast were coupled with decreases in activity of the CREB transcription factor that mediates SNS signaling through β-adrenergic receptors (Cole et al., 2010; Mayr & Montminy, 2001). On the contrary, among older adults who completed biofeedback training, we did not observe training effects on LC contrast. Thus, for younger adults, using biofeedback to increase heart rate oscillations in daily training sessions affected LC MRI contrast.

Why might HRV biofeedback training have decreased LC contrast in younger adults? The beneficial effects of HRV biofeedback involving slow breathing are thought to occur through multiple mechanisms, including stimulation of the vagus nerve (Huang et al., 2018; Lehrer & Gevirtz, 2014). The vagus nerve is a major component of the parasympathetic nervous system and sends inputs to the LC via the medullary NTS (Badran et al., 2018; Fornai et al., 2011). The NTS is affected by respiration, with NTS cell firing suppressed during inhalation and facilitated during exhalation (Miyazaki et al., 1998). Thus, the two respiratory phases may affect LC activity differently. In support of this idea, exhalation-gated auricular vagal afferent nerve stimulation elicits greater responses in NTS and LC compared to inhalation-gated stimulation in humans (Garcia et al., 2017; Sclocco et al., 2019). Slow-paced breathing increases the amplitude of oscillations in lung volume and blood pressure (Barnett et al., 2020; Russo et al., 2017) and should therefore increase the amplitude of oscillations in stretch receptor inputs from the lungs and blood vessels to the vagus nerve. Thus, one possibility is thus that the repeated practice of slow, paced breathing promotes phasic while disrupting tonic LC activity. In addition, a cluster of

neurons in the medullary preBötzinger complex serves as a major breathing rhythm generator and provides excitatory input to the LC; when breathing is slow, the preBötzinger cluster provides less excitatory input to the LC, promoting lower tonic levels of arousal (Yackle et al., 2017). These slow-breathing effects would have the net effect of shifting LC activity to a higher phasic and lower tonic level, which would manifest as lower LC MRI signal contrast and reduced sympathetic activity. The association we observed between decreases in LC contrast and decreases in activity of the CREB transcription factor are consistent with the notion of decreased LC contrast in younger adults reflecting decreased cumulative noradrenergic activity during the intervention time frame.

More broadly, our effects may be accounted for by an overall shift to parasympathetic dominance that occurs with the repeated practice of HRV biofeedback training. The LC receives projections from the medulla's nucleus paragigantocellularis (Aston-Jones et al., 1986; Aston-Jones et al., 1991), which itself receives widespread autonomic inputs and has been implicated in the regulation and control of sympathetic activity and respiration (Van Bockstaele & Aston-Jones, 1995). Parasympathetic/sympathetic balance is then expected to directly impact the LC. As correlational evidence for this idea in humans, we previously found that HRV was negatively associated with LC MRI contrast in younger adults (Mather et al., 2017). In addition, LC efferent projections provide excitatory control over preganglionic sympathetic neurons and inhibitory control over the parasympathetic dorsal motor vagal nucleus and nucleus ambiguus (Samuels & Szabadi, 2008). Having relatively lower LC structural integrity would therefore give rise to less excitatory input to sympathetic centers and reduced inhibition of parasympathetic centers, as well as reduced excitatory input to the central nucleus of the amygdala by LC neurons, which also contribute to sympathetic activation (Wood et al., 2017).

We found that the effects of biofeedback were larger for the left than the right LC. Decreases in LC contrast for participants in the Osc+ condition were greater for the left than the right LC, and significant associations with training oscillatory power and CREB activity were observed for the left, but not the right, LC. Previous studies have reported higher MRI-assessed LC integrity in the left compared to the right LC (Betts et al., 2017; Dahl et al., 2019; Galgani et al., 2023; Giorgi et al., 2022; Liu et al., 2019). Our findings are also in line with reports of more positive associations between LC contrast and cortical thickness for left relative to right LC (Bachman et al., 2021), as well as hemispheric differences in functional connectivity of the LC (Jacobs et al., 2018).

We also observed sex differences in how training oscillatory power related to change in LC contrast among younger participants, with males exhibiting a more negative association between training power and change in LC contrast than females. Relative to that of males, the female LC exhibits morphological and functional differences: LC neurons are more sensitive to corticotropin releasing factor (Bangasser et al., 2016) and exhibit greater dendritic density and branching (Bangasser et al., 2011; Ross & Van Bockstaele, 2020) in females. In line with previous reports of higher MRI-assessed measures of LC integrity in females than males (Bachman et al., 2021; Galgani et al., 2023; Riphagen et al., 2020), we found that younger females had higher LC contrast than males across conditions, hemispheres and timepoints. Our findings of change being more coupled with training oscillatory power in younger males than females suggests that there are sex differences in the factors that shape LC contrast over time, which warrants further investigation.

Although we observed differential effects of the two HRV biofeedback training conditions on LC contrast among younger participants, this was not the case among older participants. Instead, among older participants, there was an overall increase in LC contrast from pre- to post-

training. The similar changes seen across the two conditions raise the possibility that older adults' LC contrast levels were sensitive to an aspect of the intervention not explored here and present in both training conditions. Yet the older cohort was small in size and mostly female and may not have been sufficiently powered to detect condition-specific effects. It is also possible that baseline differences in stress or emotional well-being between the younger and older adults contributed to the age differences in the impact of the interventions on LC contrast. The lack of condition effects we observed for older participants should therefore be interpreted with caution.

There are several other limitations to note. First, RNA sequencing analyses included only a subset of younger participants as we started collecting blood samples after some participants had completed the study. In addition, activity of the CREB transcription factor is not a direct measure of noradrenergic activity. Second, participants in this study included mostly university students, limiting the external validity of results and potentially introducing a secular trend towards greater SNS activity as the 7-week study progressed; we aimed to avoid semester breaks in the study and therefore, across conditions, enrolled most younger participants at the beginning of semesters, when there are usually fewer exams and deadlines relative to later weeks in the semester.

Another limitation is that we did not test the reliability of the LC contrast measure within the context of our study. However, we previously found an ICC of 0.87 for LC contrast measured with a similar sequence (Dahl et al., 2019, see Supplementary Information p. 15-16), and other published studies indicate moderate-to-high reliability of LC contrast (Betts et al., 2017; Langley et al., 2017; Tona et al., 2017). Another limitation is that, while the older adults in this study were living independently in the community and had TELE scores ≥16, we did not employ more sensitive cognitive screening. The TELE screens for possible dementia using a brief telephone-based assessment but it does not rule out potential mild cognitive impairment. Thus, our older

cohort may have included participants with mild cognitive impairment, which could have affected results. For instance, greater levels of Alzheimer's disease pathology in the LC may decrease its sensitivity to interventions such as heart rate variability biofeedback.

We hope that some of the questions raised by our study can be addressed in future research. For instance, our study was not well-suited to examine the relationship between changes in anxiety and changes in LC MRI contrast, as our previously published findings with younger participants indicated that participants expected both interventions to improve their well-being (Nashiro et al., 2023). While it was a strength of our study that the comparison group yielded similar expectations, the expectations that the interventions would have positive effects may have driven the decreases in negative mood and depression seen in both groups (see Nashiro et al., 2023) and may have obscured effects of the interventions themselves on self-reported mood, depression and anxiety. Meta analyses of previous studies indicate that HRV biofeedback reduces depression and anxiety (Goessl et al., 2017; Lehrer et al., 2020; Pizzoli et al., 2021), but previous studies have not had such well-matched expectations in their comparison groups so it remains to be seen how much previous findings were driven by participant expectations. In future studies, to be able to examine the role of LC contrast changes in anxiety changes, it would be helpful to avoid inducing expectations of emotional changes (by, for instance, examining these relationships in a study in which the main outcome is cognitive performance).

Another important question for future research is whether longer interventions might yield larger effects. Our study only encompassed 5 weeks of HRV biofeedback training, whereas training over longer time periods may yield larger effects on LC contrast in both hemispheres and in younger and older participants. With larger samples that provide sufficient power for mediation analyses (Fritz & MacKinnon, 2007), it would also be interesting to examine variables that might mediate changes in LC MRI contrast.

Of course, a major question to address in future research is what these changes in LC MRI contrast represent on a cellular level. As discussed in the Introduction, current research suggests that they represent some change in the macromolecular-to-free-water fraction within the LC (Priovoulos et al., 2020; Trujillo et al., 2017; Watanabe, 2022; Watanabe et al., 2019). It is possible that HRV biofeedback affects the macromolecular-to-free-water fraction within the LC by affecting LC tonic levels of activity or by affecting inflammation in this region. Future research should include additional measures to provide insight into these and other potential pathways.

5. Conclusions

In summary, in this study, we assessed the effect of performing 5 weeks of heart rate variability biofeedback training on LC contrast, a measure that has been linked to cognition in older adults and arousal and negative affect in younger adults. We found that training decreased left LC contrast among younger participants and this effect scaled with the extent to which participants increased their heart rate oscillations during training. Furthermore, decreases in left LC contrast were related to decreases in CREB activity, a marker of sympathetic nervous system activity. These results provide novel evidence that among younger adults, LC contrast can be changed through the daily practice of increasing heart rate oscillations. More generally, these results provide new evidence suggesting that autonomic activity can influence LC contrast. Understanding the relationships between autonomic activity and LC contrast is important for better understanding the underlying mechanisms that lead to low or high LC contrast in childhood and young adulthood, before Alzheimer's-disease-related pathology has had an impact.

Data and Code Availability

Data are available at: https://openneuro.org/datasets/ds003823. Code for statistical analysis is available at: https://github.com/EmotionCognitionLab/HRV-LC.

Declaration of Interest

Declarations of interest: none.

Acknowledgments

We are grateful to Sumedha Attanti and Juliana Lee who performed manual LC delineation and the following individuals who helped collect data for the project: Collin Amano, Kathryn Cassutt, Christine Cho, Paul Choi, Akanksha Jain, Katherine Jeung, Sophia Ling, Althea Wolfe, Michelle Wong, Yong Zhang, and Cyndy Zhuang. We also thank Martin Dahl for advice on LC delineation.

This work was supported by National Science Foundation grant number DGE-1842487, and by the National Institute on Aging of the National Institutes of Health under award numbers R01AG057184, P30AG017265, and T32AG000037. The content is solely the responsibility of the authors and does not necessarily represent the official views of the National Institutes of Health.

References

Aston-Jones, G., Ennis, M., Pieribone, V., Nickell, W., & Shipley, M. (1986). The brain nucleus locus coeruleus: restricted afferent control of a broad efferent network. *Science*, *234*(4777), 734–737. https://doi.org/10.1126/science.3775363

Aston-Jones, G., Shipley, M. T., Chouvet, G., Ennis, M., van Bockstaele, E., Pieribone, V., Shiekhattar, R., Akaoka, H., Drolet, G., & Astier, B. (1991). Afferent regulation of locus coeruleus neurons: Anatomy, physiology and pharmacology. *Progress in Brain Research*, *88*, 4775. https://doi.org/10.1016/s0079-6123(08)63799-1

Avants, B. B., Tustison, N. J., Song, G., Cook, P. A., Klein, A., & Gee, J. C. (2011). A reproducible evaluation of ANTs similarity metric performance in brain image registration. *NeuroImage*, *54*(3), 2033–2044. https://doi.org/10.1016/j.neuroimage.2010.09.025

Bachman, S. L., Dahl, M. J., Werkle-Bergner, M., Düzel, S., Forlim, C. G., Lindenberger, U., Kühn, S., & Mather, M. (2021). Locus coeruleus MRI contrast is associated with cortical thickness in older adults. *Neurobiology of Aging*, *100*, 72–82. https://doi.org/10.1016/j.neurobiolaging.2020.12.019

Badran, B. W., Dowdle, L. T., Mithoefer, O. J., LaBate, N. T., Coatsworth, J., Brown, J. C., DeVries, W. H., Austelle, C. W., McTeague, L. M., & George, M. S. (2018). Neurophysiologic effects of transcutaneous auricular vagus nerve stimulation (taVNS) via electrical stimulation of the tragus: A concurrent taVNS/fMRI study and review. *Brain Stimulation*, *11*(3), 492–500. https://doi.org/10.1016/j.brs.2017.12.009

Baker, K. G., Trk, I., Hornung, J.-P., & Halasz, P. (1989). The human locus coeruleus complex: An immunohistochemical and three dimensional reconstruction study. Experimental Brain Research, 77(2), 257–270. https://doi.org/10.1007/BF00274983

Bangasser, D. A., Wiersielis, K. R., & Khantsis, S. (2016). Sex differences in the locus coeruleus- system and its regulation by stress. *Brain Research*, *1641*, 177188. https://doi.org/10.1016/j.brainres.2015.11.021

Bangasser, D. A., Zhang, X., Garachh, V., Hanhauser, E., & Valentino, R. J. (2011). Sexual dimorphism in locus coeruleus dendritic morphology: A structural basis for sex differences in emotional arousal. *Physiology & Behavior*, *103*(3-4), 342–351. https://doi.org/10.1016/j.physbeh.2011.02.037

Barnett, W. H., Latash, E. M., Capps, R. A., Dick, T. E., Wehrwein, E. A., & Molkov, Y. I. (2020). Traube–Hering waves are formed by interaction of respiratory sinus arrhythmia and pulse pressure modulation in healthy men. Journal of Applied Physiology, 129(5), 1193–1202. https://doi.org/10.1152/japplphysiol.00452.2020

Bates, D., Mächler, M., Bolker, B., & Walker, S. (2015). Fitting linear mixed-effects models using lme4. *Journal of Statistical Software*, *67*(1). https://doi.org/10.18637/jss.v067.i01

Bell, T. R., Elman, J. A., Beck, A., Fennema-Notestine, C., Gustavson, D. E., Hagler, D. J., Jack, A. J., Lyons, M. J., Puckett, O. K., Toomey, R., Franz, C. E., & Kremen, W. S. (2022). Rostral-middle locus coeruleus integrity and subjective cognitive decline in early old age. *Journal of the International Neuropsychological Society*, 1–12. https://doi.org/10.1017/S1355617722000881

Ben-Shachar, M. S., Lüdecke, D., & Makowski, D. (2020). effectsize: Estimation of effect size indices and standardized parameters. *Journal of Open Source Software*, *5*(56), 2815. https://doi.org/10.21105/joss.02815

Berridge, C. W., & Waterhouse, B. D. (2003). The locus coeruleus-noradrenergic system: Modulation of behavioral state and state-dependent cognitive processes. *Brain Research Reviews*, *42*(1), 33–84. https://doi.org/10.1016/S0165-0173(03)00143-7

Betts, M. J., Cardenas-Blanco, A., Kanowski, M., Jessen, F., & Düzel, E. (2017). In vivo MRI assessment of the human locus coeruleus along its rostrocaudal extent in young and older adults. *NeuroImage*, *163*, 150–159. https://doi.org/10.1016/j.neuroimage.2017.09.042

Betts, M. J., Kirilina, E., Otaduy, M. C. G., Ivanov, D., Acosta-Cabronero, J., Callaghan, M. F., Lambert, C., Cardenas-Blanco, A., Pine, K., Passamonti, L., Loane, C., Keuken, M. C., Trujillo, P., Lüsebrink, F., Mattern, H., Liu, K. Y., Priovoulos, N., Fliessbach, K., Dahl, M. J., … Hämmerer, D. (2019). Locus coeruleus imaging as a biomarker for noradrenergic dysfunction in neurodegenerative diseases. *Brain*, *142*(9), 2558–2571. https://doi.org/10.1093/brain/awz193

Braak, H., Thal, D. R., Ghebremedhin, E., & Tredici, K. D. (2011). Stages of the pathologic process in alzheimer disease: Age categories from 1 to 100 years. *Journal of Neuropathology & Experimental Neurology*, *70*(11), 960969.

Brown, H. J., Peng, L., Harada, J. N., Walker, J. R., Cole, S., Lin, S.-F., Zack, J. A., Chanda, S. K., & Sun, R. (2010). Gene Expression and Transcription Factor Profiling Reveal Inhibition of Transcription Factor cAMP-response Element-binding Protein by γ-Herpesvirus Replication and Transcription Activator. *Journal of Biological Chemistry*, *285*(33), 25139–25153. https://doi.org/10.1074/jbc.M110.137737

Brown, R. P., & Gerbarg, P. L. (2005). Sudarshan Kriya Yogic Breathing in the Treatment of Stress, Anxiety, and Depression: Part I Neurophysiologic Model. *The Journal of Alternative and Complementary Medicine*, *11*(1), 189–201. https://doi.org/10.1089/acm.2005.11.189

Cassidy, C. M., Zucca, F. A., Girgis, R. R., Baker, S. C., Weinstein, J. J., Sharp, M. E., Bellei, C., Valmadre, A., Vanegas, N., Kegeles, L. S., Brucato, G., Kang, U. J., Sulzer, D., Zecca, L., Abi-Dargham, A., & Horga, G. (2019). Neuromelanin-sensitive MRI as a noninvasive

proxy measure of dopamine function in the human brain. Proceedings of the National Academy of Sciences, 116(11), 5108–5117. https://doi.org/10.1073/pnas.1807983116

Chalermpalanupap, T., Weinshenker, D., & Rorabaugh, J. M. (2017). Down but not out: The consequences of pretangle tau in the locus coeruleus. *Neural Plasticity*, *2017*, 19. https://doi.org/10.1155/2017/7829507

Chu, W. T., Wang, W., Zaborszky, L., Golde, T. E., DeKosky, S., Duara, R., Loewenstein, D. A., Adjouadi, M., Coombes, S. A., & Vaillancourt, D. E. (2022). Association of Cognitive Impairment With Free Water in the Nucleus Basalis of Meynert and Locus Coeruleus to Transentorhinal Cortex Tract. *Neurology*, *98*(7), e700–e710. https://doi.org/10.1212/WNL.0000000000013206

Cole, S. W., Arevalo, J. M. G., Takahashi, R., Sloan, E. K., Lutgendorf, S. K., Sood, A. K., Sheridan, J. F., & Seeman, T. E. (2010). Computational identification of gene-social environment interaction at the human IL6 locus. *Proceedings of the National Academy of Sciences*, *107*(12), 5681–5686. https://doi.org/10.1073/pnas.0911515107

Cole, S. W., Shanahan, M. J., Gaydosh, L., & Harris, K. M. (2020). Population-based RNA profiling in Add Health finds social disparities in inflammatory and antiviral gene regulation to emerge by young adulthood. *Proceedings of the National Academy of Sciences*, *117*(9), 4601–4608. https://doi.org/10.1073/pnas.1821367117

Cole, S. W., Yan, W., Galic, Z., Arevalo, J., & Zack, J. A. (2005). Expression-based monitoring of transcription factor activity: the TELiS database. *Bioinformatics (Oxford, England)*, *21*(6), 803–810. https://doi.org/10.1093/bioinformatics/bti038

Dahl, M. J., Mather, M., Düzel, S., Bodammer, N. C., Lindenberger, U., Kühn, S., & Werkle-Bergner, M. (2019). Rostral locus coeruleus integrity is associated with better memory

performance in older adults. *Nature Human Behaviour*, *3*(11), 1203–1214. https://doi.org/10.1038/s41562-019-0715-2

Dahl, M. J., Mather, M., Werkle-Bergner, M., Kennedy, B. L., Guzman, S., Hurth, K., Miller, C. A., Qiao, Y., Shi, Y., Chui, H. C., & Ringman, J. M. (2022). Locus coeruleus integrity is related to tau burden and memory loss in autosomal-dominant Alzheimer's disease. *Neurobiology of Aging*, *112*, 39–54. https://doi.org/10.1016/j.neurobiolaging.2021.11.006

Elman, J. A., Puckett, O. K., Beck, A., Fennema-Notestine, C., Cross, L. K., Dale, A. M., Eglit, G. M. L., Eyler, L. T., Gillespie, N. A., Granholm, E. L., Gustavson, D. E., Hagler, D. J., Hatton, S. N., Hauger, R., Jak, A. J., Logue, M. W., McEvoy, L. K., McKenzie, R. E., Neale, M. C., … Kremen, W. S. (2021). MRI-assessed locus coeruleus integrity is heritable and associated with multiple cognitive domains, mild cognitive impairment, and daytime dysfunction. *Alzheimer's & Dementia*, *17*, 1017–1025. https://doi.org/https://doi.org/10.1002/alz.12261

Fornai, F., Ruffoli, R., Giorgi, F. S., & Paparelli, A. (2011). The role of locus coeruleus in the antiepileptic activity induced by vagus nerve stimulation: Locus coeruleus and vagus nerve stimulation. *European Journal of Neuroscience*, *33*(12), 2169–2178. https://doi.org/10.1111/j.1460-9568.2011.07707.x

Fritz, M. S., & MacKinnon, D. P. (2007). Required sample size to detect the mediated effect. *Psychological Science*, *18*(3), 233–239. https://doi.org/10.1111/j.1467-9280.2007.01882.x

Galgani, A., Lombardo, F., Martini, N., Vergallo, A., Bastiani, L., Hampel, H., Hlavata, H., Baldacci, F., Tognoni, G., De Marchi, D., Ghicopulos, I., De Cori, S., Biagioni, F., Busceti, C. L., Ceravolo, R., Bonuccelli, U., Chiappino, D., Siciliano, G., Fornai, F., … Giorgi, F. S. (2023). Magnetic resonance imaging Locus Coeruleus abnormality in

amnestic Mild Cognitive Impairment is associated with future progression to dementia. *European Journal of Neurology*, *30*(1), 32–46. https://doi.org/10.1111/ene.15556

Garcia, R. G., Lin, R. L., Lee, J., Kim, J., Barbieri, R., Sclocco, R., Wasan, A. D., Edwards, R. R., Rosen, B. R., Hadjikhani, N., & Napadow, V. (2017). Modulation of brainstem activity and connectivity by respiratory-gated auricular vagal afferent nerve stimulation in migraine patients. *Pain*, *158*(8), 1461–1472. https://doi.org/10.1097/j.pain.0000000000000930

Gatz, M., Reynolds, C., Nikolic, J., Lowe, B., Karel, M., & Pedersen, N. (1995). An Empirical Test of Telephone Screening to Identify Potential Dementia Cases. *International Psychogeriatrics*, *7*(3), 429–438. https://doi.org/10.1017/S1041610295002171

Giorgi, F. S., Martini, N., Lombardo, F., Galgani, A., Bastiani, L., Della Latta, D., Hlavata, H., Busceti, C. L., Biagioni, F., Puglisi-Allegra, S., Pavese, N., & Fornai, F. (2022). Locus Coeruleus magnetic resonance imaging: a comparison between native-space and template-space approach. *Journal of Neural Transmission*, *129*(4), 387–394. https://doi.org/10.1007/s00702-022-02486-5

Goessl, V. C., Curtiss, J. E., & Hofmann, S. G. (2017). The effect of heart rate variability biofeedback training on stress and anxiety: A meta-analysis. *Psychological Medicine*, *47*(15), 25782586. https://doi.org/10.1017/S0033291717001003

Hämmerer, D., Callaghan, M. F., Hopkins, A., Kosciessa, J., Betts, M., Cardenas-Blanco, A., Kanowski, M., Weiskopf, N., Dayan, P., Dolan, R. J., & Düzel, E. (2018). Locus coeruleus integrity in old age is selectively related to memories linked with salient negative events. *Proceedings of the National Academy of Sciences*, *115*(9), 2228–2233. https://doi.org/10.1073/pnas.1712268115

Harley, C. W., Walling, S. G., Yuan, Q., & Martin, G. M. (2021). The ‘a, b, c’s of pretangle tau and their relation to aging and the risk of Alzheimer’s Disease. *Seminars in Cell & Developmental Biology*, *116*, 125–134. https://doi.org/10.1016/j.semcdb.2020.12.010

Harley, C. W., & Yuan, Q. (2021). Locus coeruleus optogenetic modulation: Lessons learned from temporal patterns. *Brain Sciences*, *11*(12), 1624. https://doi.org/10.3390/brainsci11121624

He, N., Chen, Y., LeWitt, P. A., Yan, F., & Haacke, E. M. (2022). Response to “Neuromelanin? MRI of Noradrenergic and Dopaminergic Neurons.” *Journal of Magnetic Resonance Imaging, jmri.28481*. https://doi.org/10.1002/jmri.28481

Huang, C., Gevirtz, R. N., Onton, J., & Criado, J. R. (2018). Investigation of vagal afferent functioning using the Heartbeat Event Related Potential. *International Journal of Psychophysiology*, *131*, 113–123. https://doi.org/10.1016/j.ijpsycho.2017.06.007

Jacobs, H. I. L., Becker, J. A., Kwong, K., Engels-Domínguez, N., Prokopiou, P. C., Papp, K. V., Properzi, M., Hampton, O. L., d’Oleire Uquillas, F., Sanchez, J. S., Rentz, D. M., El Fakhri, G., Normandin, M. D., Price, J. C., Bennett, D. A., Sperling, R. A., & Johnson, K. A. (2021). In vivo and neuropathology data support locus coeruleus integrity as indicator of alzheimer’s disease pathology and cognitive decline. *Science Translational Medicine*, *13*(612), eabj2511. https://doi.org/10.1126/scitranslmed.abj2511

Jacobs, H. I. L., Müller-Ehrenberg, L., Priovoulos, N., & Roebroeck, A. (2018). Curvilinear locus coeruleus functional connectivity trajectories over the adult lifespan: A 7T MRI study. *Neurobiology of Aging*, *69*, 167–176. https://doi.org/10.1016/j.neurobiolaging.2018.05.021

Jester, D. J., Rozek, E. K., & McKelley, R. A. (2019). Heart rate variability biofeedback: Implications for cognitive and psychiatric effects in older adults. *Aging & Mental Health*, *23*(5), 574580. https://doi.org/10.1080/13607863.2018.1432031

Keren, N. I., Taheri, S., Vazey, E. M., Morgan, P. S., Granholm, A.-C. E., Aston-Jones, G. S., & Eckert, M. A. (2015). Histologic validation of locus coeruleus MRI contrast in post-mortem tissue. NeuroImage, 113, 235–245. https://doi.org/10.1016/j.neuroimage.2015.03.020

Kitao, S., Matsusue, E., Fujii, S., Miyoshi, F., Kaminou, T., Kato, S., Ito, H., & Ogawa, T. (2013). Correlation between pathology and neuromelanin MR imaging in Parkinson's disease and dementia with Lewy bodies. Neuroradiology, 55(8), 947–953. https://doi.org/10.1007/s00234-013-1199-9

Kuznetsova, A., Brockhoff, P. B., & Christensen, R. H. B. (2017). lmerTest package: Tests in linear mixed effects models. *Journal of Statistical Software*, *82*(13). https://doi.org/10.18637/jss.v082.i13

Langley, J., Huddleston, D. E., Liu, C. J., & Hu, X. (2017). Reproducibility of locus coeruleus and substantia nigra imaging with neuromelanin sensitive MRI. Magnetic Resonance Materials in Physics, Biology and Medicine, 30(2), 121–125. https://doi.org/10.1007/s10334-016-0590-z

Lehrer, P. M., & Gevirtz, R. (2014). Heart rate variability biofeedback: How and why does it work? *Frontiers in Psychology*, *5*. https://doi.org/10.3389/fpsyg.2014.00756

Lehrer, P., Kaur, K., Sharma, A., Shah, K., Huseby, R., Bhavsar, J., Sgobba, P., & Zhang, Y. (2020). Heart Rate Variability Biofeedback Improves Emotional and Physical Health and Performance: A Systematic Review and Meta Analysis. *Applied Psychophysiology and Biofeedback*, *45*(3), 109–129. https://doi.org/10.1007/s10484-020-09466-z

Lehrer, P. M., Vaschillo, E., Vaschillo, B., Lu, S.-E., Eckberg, D. L., Edelberg, R., Shih, W. J., Lin, Y., Kuusela, T. A., Tahvanainen, K. U. O., & Hamer, R. M. (2003). Heart rate variability biofeedback increases baroreflex gain and peak expiratory flow. *Psychosomatic Medicine*, *65*(5), 796805. https://doi.org/10.1097/01.PSY.0000089200.81962.19

Lenth, R. V. (2021). *Emmeans: Estimated marginal means, aka least-squares means*. https://CRAN.R-project.org/package=emmeans

Liu, K. Y., Acosta-Cabronero, J., Cardenas-Blanco, A., Loane, C., Berry, A. J., Betts, M. J., Kievit, R. A., Henson, R. N., Düzel, E., Howard, R., & Hämmerer, D. (2019). In vivo visualization of age-related differences in the locus coeruleus. *Neurobiology of Aging*, *74*, 101–111. https://doi.org/10.1016/j.neurobiolaging.2018.10.014

Liu, K. Y., Kievit, R. A., Tsvetanov, K. A., Betts, M. J., Düzel, E., Rowe, J. B., Howard, R., & Hämmerer, D. (2020). Noradrenergic-dependent functions are associated with age-related locus coeruleus signal intensity differences. *Nature Communications*, *11*(1), 1712. https://doi.org/10.1038/s41467-020-15410-w

Liu, K. Y., Marijatta, F., Hämmerer, D., Acosta-Cabronero, J., Düzel, E., & Howard, R. J. (2017). Magnetic resonance imaging of the human locus coeruleus: A systematic review. *Neuroscience & Biobehavioral Reviews*, *83*, 325–355. https://doi.org/10.1016/j.neubiorev.2017.10.023

Lorton, D., & Bellinger, D. (2015). Molecular mechanisms underlying β-Adrenergic receptor-mediated cross-talk between sympathetic neurons and immune cells. *International Journal of Molecular Sciences*, *16*(12), 5635–5665. https://doi.org/10.3390/ijms16035635

Luckey, A. M., Robertson, I. H., Lawlor, B., Mohan, A., & Vanneste, S. (2021). Sex differences in locus coeruleus: A heuristic approach that may explain the increased risk of

Alzheimer's disease in females. *Journal of Alzheimer's Disease*, *83*(2), 505–522. https://doi.org/10.3233/JAD-210404

MacAulay, N. (2021). Molecular mechanisms of brain water transport. Nature Reviews Neuroscience, 22(6), 326–344. https://doi.org/10.1038/s41583-021-00454-8

Mather, M., Joo Yoo, H., Clewett, D. V., Lee, T.-H., Greening, S. G., Ponzio, A., Min, J., & Thayer, J. F. (2017). Higher locus coeruleus MRI contrast is associated with lower parasympathetic influence over heart rate variability. *NeuroImage*, *150*, 329–335. https://doi.org/10.1016/j.neuroimage.2017.02.025

Mayr, B., & Montminy, M. (2001). Transcriptional regulation by the phosphorylation-dependent factor CREB. *Nature Reviews Molecular Cell Biology*, *2*(8), 599–609. https://doi.org/10.1038/35085068

McCall, Jordan G., Al-Hasani, R., Siuda, Edward R., Hong, Daniel Y., Norris, Aaron J., Ford, Christopher P., & Bruchas, Michael R. (2015). CRH engagement of the locus coeruleus noradrenergic system mediates stress-induced anxiety. *Neuron*, *87*(3), 605–620. https://doi.org/10.1016/j.neuron.2015.07.002

Miyazaki, M., Arata, A., Tanaka, I., & Ezure, K. (1998). Activity of rat pump neurons is modulated with central respiratory rhythm. *Neuroscience Letters*, *249*(1), 61–64. https://doi.org/10.1016/S0304-3940(98)00402-9

Morris, L. S., Tan, A., Smith, D. A., Grehl, M., Han-Huang, K., Naidich, T. P., … Kundu, P. (2020). Sub-millimeter variation in human locus coeruleus is associated with dimensional measures of psychopathology: An in vivo ultra-high field 7-Tesla MRI study. *NeuroImage: Clinical*, *25*(September 2019), 102148. https://doi.org/10.1016/j.nicl.2019.102148

Mulcahy, J. S., Larsson, D. E. O., Garfinkel, S. N., & Critchley, H. D. (2019). Heart rate variability as a biomarker in health and affective disorders: A perspective on neuroimaging studies. *NeuroImage*, *202*, 116072. https://doi.org/10.1016/j.neuroimage.2019.116072

Nashiro, K., Min, J., Yoo, H. J., Cho, C., Bachman, S. L., Dutt, S., Thayer, J. F., Lehrer, P. M., Feng, T., Mercer, N., Nasseri, P., Wang, D., Chang, C., Marmarelis, V. Z., Narayanan, S., Nation, D. A., & Mather, M. (2023). Increasing coordination and responsivity of emotion-related brain regions with a heart rate variability biofeedback randomized trial. Cognitive, Affective, & Behavioral Neuroscience, *23, 66-83*. https://doi.org/10.3758/s13415-022-01032-w

Østby, I., Øyehaug, L., Einevoll, G. T., Nagelhus, E. A., Plahte, E., Zeuthen, T., Lloyd, C. M., Ottersen, O. P., & Omholt, S. W. (2009). Astrocytic mechanisms explaining neural-activity-induced shrinkage of extraneuronal space. PLoS Computational Biology, 5(1), e1000272. https://doi.org/10.1371/journal.pcbi.1000272

Pizzoli, S. F. M., Marzorati, C., Gatti, D., Monzani, D., Mazzocco, K., & Pravettoni, G. (2021). A meta-analysis on heart rate variability biofeedback and depressive symptoms. *Scientific Reports*, *11*(1), 6650. https://doi.org/10.1038/s41598-021-86149-7

Powell, N. D., Sloan, E. K., Bailey, M. T., Arevalo, J. M. G., Miller, G. E., Chen, E., Kobor, M. S., Reader, B. F., Sheridan, J. F., & Cole, S. W. (2013). Social stress up-regulates inflammatory gene expression in the leukocyte transcriptome via -adrenergic induction of myelopoiesis. *Proceedings of the National Academy of Sciences*, *110*(41), 16574–16579. https://doi.org/10.1073/pnas.1310655110

Priovoulos, N., van Boxel, S. C. J., Jacobs, H. I. L., Poser, B. A., Uludag, K., Verhey, F. R. J., & Ivanov, D. (2020). Unraveling the contributions to the neuromelanin-MRI contrast. Brain Structure and Function, 225(9), 2757–2774. https://doi.org/10.1007/s00429-020-02153-z

R Core Team. (2021). *R: A language and environment for statistical computing*. R Foundation for Statistical Computing. https://www.R-project.org/

Rajkowska, G. & Goldman-Rakic, P. S. (1995). Cytoarchitectonic Definition of Prefrontal Areas in the Normal Human Cortex: I. Remapping of Areas 9 and 46 using Quantitative Criteria. Cerebral Cortex, 5(4), 307–322. https://doi.org/10.1093/cercor/5.4.307

Ramon-Moliner, E. (1974). The locus coeruleus of cat: III. Light and electron microscopic studies. Cell and Tissue Research, 149(2). https://doi.org/10.1007/BF00222274

Riphagen, J. M., Hooren, R. W. E. van, Pagen, L. H. G., Poser, B. A., & Jacobs, H. I. L. (2020). Rostro-caudal locus coeruleus integrity differences vary with age and sex using ultra-high field imaging: Neuroimaging / Optimal neuroimaging measures for early detection. *Alzheimer's & Dementia*, *16*(S5). https://doi.org/10.1002/alz.046722

Roseboom, P. H., & Klein, D. C. (1995). Norepinephrine stimulation of pineal cyclic AMP response element-binding protein phosphorylation: Primary role of a beta-adrenergic receptor/cyclic AMP mechanism. *Molecular Pharmacology*, *47*(3), 439–449.

Ross, J. A., & Van Bockstaele, E. J. (2020). The role of catecholamines in modulating responses to stress: Sex-specific patterns, implications, and therapeutic potential for post-traumatic stress disorder and opiate withdrawal. *European Journal of Neuroscience*, *215*, ejn.14714. https://doi.org/10.1111/ejn.14714

Russo, M. A., Santarelli, D. M., & O'Rourke, D. (2017). The physiological effects of slow breathing in the healthy human. Breathe, 13(4), 298–309. https://doi.org/10.1183/20734735.009817

Samuels, E., & Szabadi, E. (2008). Functional neuroanatomy of the noradrenergic locus coeruleus: Its roles in the regulation of arousal and autonomic function part I: Principles of functional organisation. *Current Neuropharmacology*, *6*(3), 235–253. https://doi.org/10.2174/157015908785777229

Sara, S. J. (2009). The locus coeruleus and noradrenergic modulation of cognition. *Nature Reviews Neuroscience*, *10*(3), 211–223. https://doi.org/10.1038/nrn2573

Sasaki, M., Shibata, E., Tohyama, K., Takahashi, J., Otsuka, K., Tsuchiya, K., Takahashi, S., Ehara, S., Terayama, Y., & Sakai, A. (2006). Neuromelanin magnetic resonance imaging of locus ceruleus and substantia nigra in parkinson's disease. *Neuroreport*, *17*(11), 1215–1218. https://doi.org/10.1097/01.wnr.0000227984.84927.a7

Schwarz, L. A., & Luo, L. (2015). Organization of the locus coeruleus-norepinephrine system. *Current Biology*, *25*(21), R1051–6. https://doi.org/10.1016/j.cub.2015.09.039

Sclocco, R., Garcia, R. G., Kettner, N. W., Isenburg, K., Fisher, H. P., Hubbard, C. S., Ay, I., Polimeni, J. R., Goldstein, J., Makris, N., Toschi, N., Barbieri, R., & Napadow, V. (2019). The influence of respiration on brainstem and cardiovagal response to auricular vagus nerve stimulation: A multimodal ultrahigh-field (7T) fMRI study. *Brain Stimulation*, *12*(4), 911–921. https://doi.org/10.1016/j.brs.2019.02.003

Shaywitz, A. J., & Greenberg, M. E. (1999). CREB: A Stimulus-Induced Transcription Factor Activated by A Diverse Array of Extracellular Signals. *Annual Review of Biochemistry*, *68*(1), 821–861. https://doi.org/10.1146/annurev.biochem.68.1.821

Sherpa, A. D., Xiao, F., Joseph, N., Aoki, C., & Hrabetova, S. (2016). Activation of β-adrenergic receptors in rat visual cortex expands astrocytic processes and reduces extracellular space volume: ECS AND ASTROCYTES DURING βAR ACTIVATION. Synapse, 70(8), 307–316. https://doi.org/10.1002/syn.21908

Thayer, J. F., & Lane, R. D. (2009). Claude Bernard and the heartbrain connection: Further elaboration of a model of neurovisceral integration. *Neuroscience & Biobehavioral Reviews*, *33*(2), 8188. https://doi.org/10.1016/j.neubiorev.2008.08.004

Thayer, J. F., & Lane, R. D. (2000). A model of neurovisceral integration in emotion regulation and dysregulation. *Journal of Affective Disorders*, *61*(3), 20116. https://doi.org/10.1016/s0165-0327(00)00338-4

Thonberg, H., Fredriksson, J. M., Nedergaard, J., & Cannon, B. (2002). A novel pathway for adrenergic stimulation of cAMP-response-element-binding protein (CREB) phosphorylation: Mediation via α1-adrenoceptors and protein kinase C activation. *Biochemical Journal*, *364*(1), 73–79. https://doi.org/10.1042/bj3640073

Tona, K.-D., Keuken, M. C., de Rover, M., Lakke, E., Forstmann, B. U., Nieuwenhuis, S., & van Osch, M. J. P. (2017). In vivo visualization of the locus coeruleus in humans: Quantifying the test–retest reliability. Brain Structure and Function, 222(9), 4203–4217. https://doi.org/czz

Trujillo, P., Summers, P. E., Ferrari, E., Zucca, F. A., Sturini, M., Mainardi, L. T., Cerutti, S., Smith, A. K., Smith, S. A., Zecca, L., & Costa, A. (2017). Contrast mechanisms associated with neuromelanin-MRI. Magnetic Resonance in Medicine, 78(5), 1790–1800. https://doi.org/10.1002/mrm.26584

Trujillo, P., Petersen, K. J., Cronin, M. J., Lin, Y.-C., Kang, H., Donahue, M. J., Smith, S. A., & Claassen, D. O. (2019). Quantitative magnetization transfer imaging of the human locus coeruleus. *NeuroImage*, *200*, 191–198. https://doi.org/10.1016/j.neuroimage.2019.06.049

Van Bockstaele, E. J., & Aston-Jones, G. (1995). Integration in the ventral medulla and coordination of sympathetic, pain and arousal functions. *Clinical and Experimental*

Hypertension (New York, N.Y.: 1993), *17*(1-2), 153–165. https://doi.org/10.3109/10641969509087062

Watanabe, T. (2022). Neuromelanin? MRI of Noradrenergic and Dopaminergic Neurons. Journal of Magnetic Resonance Imaging, jmri.28479. https://doi.org/10.1002/jmri.28479

Watanabe, T., Wang, X., Tan, Z., & Frahm, J. (2019). Magnetic resonance imaging of brain cell water. Scientific Reports, 9(1), 1–14. https://doi.org/10.1038/s41598-019-41587-2

Weber, C. S., Thayer, J. F., Rudat, M., Wirtz, P. H., Zimmermann-Viehoff, F., Thomas, A., Perschel, F. H., Arck, P. C., & Deter, H. C. (2010). Low vagal tone is associated with impaired post stress recovery of cardiovascular, endocrine, and immune markers. *European Journal of Applied Physiology*, *109*(2), 201211. https://doi.org/10.1007/s00421-009-1341-x

Wilson, R. S., Nag, S., Boyle, P. A., Hizel, L. P., Yu, L., Buchman, A. S., Schneider, J. A., & Bennett, D. A. (2013). Neural reserve, neuronal density in the locus ceruleus, and cognitive decline. *Neurology*, *80*(13), 1202–1208. https://doi.org/10.1212/WNL.0b013e3182897103

Wood, C. S., Valentino, R. J., & Wood, S. K. (2017). Individual differences in the locus coeruleus-norepinephrine system: Relevance to stress-induced cardiovascular vulnerability. *Physiology & Behavior*, *172*, 40–48. https://doi.org/10.1016/j.physbeh.2016.07.008

Xie, L., Kang, H., Xu, Q., Chen, M. J., Liao, Y., Thiyagarajan, M., O'Donnell, J., Christensen, D. J., Nicholson, C., Iliff, J. J., Takano, T., Deane, R., & Nedergaard, M. (2013). Sleep Drives Metabolite Clearance from the Adult Brain. Science, 342(6156), 373–377. https://doi.org/10.1126/science.1241224

Yackle, K., Schwarz, L. A., Kam, K., Sorokin, J. M., Huguenard, J. R., Feldman, J. L., Luo, L., & Krasnow, M. A. (2017). Breathing control center neurons that promote arousal in mice. *Science*, *355*(6332), 14111415. https://doi.org/10.1126/science.aai7984

Ycaza Herrera, A., Wang, J., & Mather, M. (2019). The gist and details of sex differences in cognition and the brain: How parallels in sex differences across domains are shaped by the locus coeruleus and catecholamine systems. *Progress in Neurobiology*, *176*, 120–133. https://doi.org/10.1016/j.pneurobio.2018.05.005

Ye, R., Rua, C., O'Callaghan, C., Jones, P. S., Hezemans, F. H., Kaalund, S. S., Tsvetanov, K. A., Rodgers, C. T., Williams, G., Passamonti, L., & Rowe, J. B. (2021). An in vivo probabilistic atlas of the human locus coeruleus at ultra-high field. *NeuroImage*, *225*, 117487. https://doi.org/10.1016/j.neuroimage.2020.117487

Ye, R., O'Callaghan, C., Rua, C., Hezemans, F. H., Holland, N., Malpetti, M., Jones, P. S., Barker, R. A., Williams-Gray, C. H., Robbins, T. W., Passamonti, L., & Rowe, J. (2022). Locus Coeruleus Integrity from 7 T MRI Relates to Apathy and Cognition in Parkinsonian Disorders. *Movement Disorders*, *37*(8), 1663–1672. https://doi.org/10.1002/mds.29072

Yoo, H. J., Nashiro, K., Min, J., Cho, C., Bachman, S. L., Nasseri, P., Porat, S., Dutt, S., Grigoryan, V., Choi, P., Thayer, J. F., Lehrer, P. M., Chang, C., & Mather, M. (2022). Heart rate variability (HRV) changes and cortical volume changes in a randomized trial of five weeks of daily HRV biofeedback in younger and older adults. *International Journal of Psychophysiology*, *181*, 50–63. https://doi.org/10.1016/j.ijpsycho.2022.08.006

Yoo, H. J., Nashiro, K., Min, J., Cho, C., Mercer, N., Bachman, S. L., Nasseri, P., Dutt, S., Porat, S., Choi, P., Zhang, Y., Grigoryan, V., Feng, T., Thayer, J. F., Lehrer, P., Chang, C., Stanley, J. A., Head, E., Rouanet, J., … Mather, M. (2023). Multimodal neuroimaging

data from a 5-week heart rate variability biofeedback randomized clinical trial. *Scientific Data*, *10*(1), 503. https://doi.org/10.1038/s41597-023-02396-5

Yushkevich, P. A., Piven, J., Hazlett, H. C., Smith, R. G., Ho, S., Gee, J. C., & Gerig, G. (2006). User-guided 3D active contour segmentation of anatomical structures: Significantly improved efficiency and reliability. *NeuroImage*, *31*(3), 1116–1128. https://doi.org/10.1016/j.neuroimage.2006.01.015

Supplementary Material: Daily heart rate variability biofeedback training decreases locus coeruleus MRI contrast in younger adults in a randomized clinical trial

Shelby L. Bachman[a], Steve Cole[b], Hyun Joo Yoo[a], Kaoru Nashiro[a], Jungwon Min[a], Noah Mercer[a], Padideh Nasseri[a], Julian F. Thayer[c], Paul Lehrer[d], & Mara Mather[a]

[a]University of Southern California

[b]University of California, Los Angeles

[c]University of California, Irvine

[d]Rutgers University

Supplementary Methods

Section 1. Details of included and excluded TSE scans

A total of 115 younger (60 Osc+, 55 Osc-) and 60 older (31 Osc+, 29 Osc-) participants pre- and/or post-training MRI assessments including a TSE scan. Of these, 15 younger and 9 older participants did not finish the study and thus did not complete a post-training MRI assessment. The proportion of participants who did not complete the study was higher for older than for younger adults because we terminated the study early due to the COVID-19 pandemic; at that point, 6 older participants were unable to complete the study. There was 1 older adult participant whose pre-training MRI assessment did not include a TSE scan. A breakdown of MRI assessments that included MPRAGE and TSE scans, according to age group, training condition and timepoint, is provided in Table S1.

Table S1:

Description of MRI assessments that included MPRAGE and TSE scans.

Age group	Training condition	Timepoint	Number of assessments
Younger	Osc+	Pre-training	60
Younger	Osc+	Post-training	52
Younger	Osc-	Pre-training	55
Younger	Osc-	Post-training	48
Older	Osc+	Pre-training	31
Older	Osc+	Post-training	26
Older	Osc-	Pre-training	28
Older	Osc-	Post-training	25

Note. Osc+ = increase-oscillations condition; Osc- = decrease-oscillations condition.

Available TSE scans were visually inspected by one trained researcher for quality and artifact. Scans with incorrect positioning (n = 3), different resolution (n = 1), or susceptibility artifact overlapping the LC or central pons (n = 5) were excluded from LC delineation. Of remaining scans, 29 were excluded due to excessive motion. As a validation step, we compared whether scans were included or excluded with qualitative information provided by two raters during manual LC delineation (Section 3); specifically, in some cases, one or both raters reported not being able to manually identify or delineate the LC due to artifact. Scans that could not be rated by either rater were considered non-rateable, whereas scans rated by at least one rater were considered rateable. We then found 93.7% agreement between whether scans had been flagged as included or excluded based on visual inspection, and their rateability. Because raters were told to prioritize delineating the LC even if the surrounding image contained excessive motion or artifact, inclusions and exclusions from visual inspection were taken as final decisions.

Section 2. LC delineation parameters and validation

We first upsampled available MPRAGE and FSE scans to twice their native resolution. For this step, the ResampleImage ANTs routine was used, using linear interpolation and pixel type set to 'float.'

We then generated an initial, whole-brain template using a subset of 134 upsampled MPRAGE scans whose fields of view were spatially well-aligned, specifically with `qoffset_x`, `qoffset_y`, and `qoffset_z` values falling within 1 standard deviation of the mean across scans. The subset included scans from 88 younger and 46 older participants. These scans were used as inputs to a run of the antsMultivariateTemplateConstruction.sh routine with the following parameters: gradient step size = 0.25, iteration limit = 6, max iterations = 1x0x0, modality weights used in similarity metric = 1, number of modalities = 1, N4 bias field correction on, rigid

body registration of inputs on, registration similarity metric = cross-correlation, transformation model type = greedy-SyN, update template with full affine transform on, no initial template. The resulting template was used as the initial template for a full template-building run of the antsMultivariateTemplateConstruction.sh routine, using all 287 (191 younger, 96 older) MPRAGE scans as inputs. This template-building run had the same parameters as the initial template-building run, except for the following: max iterations = 30x90x20, rigid body registration of inputs off. The result was a full, whole-brain (MPRAGE) template, as well as each inputted MPRAGE scan coregistered to whole-brain template space.

Coregistration of upsampled TSE scans to corresponding whole-brain template-coregistered MPRAGE scans was performed using antsRegistrationSyNQuick.sh, with the following parameters: transform type = rigid, affine and deformable SyN ('s'), histogram bins = 32, spline distance = 26, precision type = double, transform type = SyN, histogram matching on. Coregistered TSE scans were then used to create a TSE template. Parameters for this template-building procedure were the same as that for the whole-brain template building procedure, except that all coregistered TSE scans were used for both the initial and full template-building runs.

We then coregistered the full TSE template with the whole-brain template, and we coregistered the whole-brain template with the MNI152 0.5mm (linear) brain. For both coregistration steps, the antsRegistrationSyN.sh routine was used with the following parameters: transform type = rigid, affine and deformable SyN ('s'), radius = 4, spline_distance = 26, precision type = double, histogram matching on, collapse output transforms on. For coregistration of the TSE template to MPRAGE template space, a binarized lesion mask was used which was constructed by thresholding the TSE template at intensity 1. Finally, using transforms from all steps above, we warped upsampled TSE scans to MNI152 0.5mm (linear) space, using the antsApplyTransforms.sh routine, with interpolation type set to linear. The

antsApplyTransforms.sh, with the same parameters, was used to apply relevant transforms to warp the TSE template to MNI152 space.

As a validation step, hyperintensities on the TSE template that had been warped to MNI152 space were compared with the locations of a publicly available LC meta-map (Dahl et al., 2022). These hyperintensities are displayed alongside the meta-map coordinates in Figure S1.

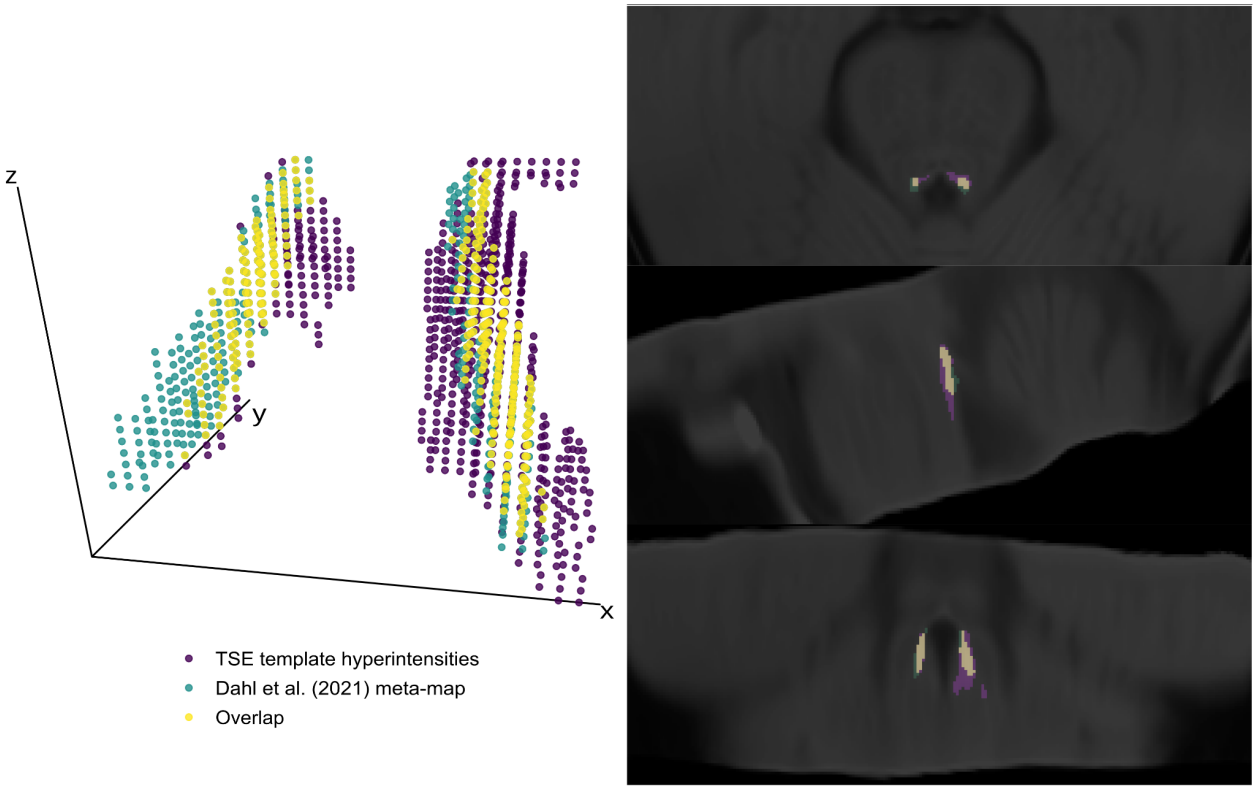

Figure S1. Comparison of signal hyperintensity locations on the TSE template, LC meta-map from Dahl et al. (2022), and their overlap. The TSE template was warped to MNI152 0.5mm (linear) standard space. Locations of hyperintensity were all voxels in the dorsal pons that survived thresholding based on intensities within the central pontine reference region. Specifically, the Dahl et al. (2022) reference map was applied as a mask to the TSE template. For each slice in the *z*-direction (*z*= 85-112), an intensity threshold was computed as the mean reference intensity in that slice plus 3.5 times the standard deviation of the reference intensity in that slice. Then, voxels within the same slice of the dorsal pons (*x* = 164-196, *y* = 174-182) where

intensities were greater than the threshold value were classified as hyperintensities. Left panel shows graphical comparison of meta-mask, template hyperintensities, and their overlap. Right panel shows the same comparison overlaid on the TSE template in MNI space (x = 187, y = 179, z = 98).

Section 3. Manual LC delineation

As a validation step, peak LC locations were also manually delineated on native-resolution TSE scans by two trained raters. Raters were blind to training condition, age and timepoint. Manual LC delineation was performed using ImageJ (Version 1.5.2, Schneider et al., 2012, https://imagej.nih.gov). according to the protocol described by Dahl et al. (2019). In summary, raters identified 2x2 voxel regions of interest in the left and right hemispheres which exhibited peak intensity and overlapped the expected location of the LC. This procedure was performed by each rater for each *z*-slice in which the left and/or right LC was visible.

For each rater, the voxel with peak LC intensity was then selected across *z*-slices, for each hemisphere separately. We then used two-way mixed-effects intra-class correlation analyses based on absolute agreement to assess correspondence between peak left and right LC intensity values across raters. These analyses indicated high correspondence between raters for the left LC ($ICC(3, 1) = 0.966$, *95% CI* = 0.951 - 0.975, $p < .001$) and right LC ($ICC(3, 1) = 0.968$, *95% CI* =0.958 - 0.976, $p < .001$). Therefore, we averaged left and right LC intensity values across raters. The resulting averaged values were used to assess correspondence between intensity values determined manually and using the semi-automated method (main text, Section 2.5.1).

Section 4. Testing for training effects on caudal and rostral LC contrast

To test for training effects on caudal and rostral LC contrast, we fit a series of linear mixed effects models. These models assessed the fixed effects of timepoint, training condition, age group, and their interactions on each rostral and caudal LC contrast. Pairwise comparisons were performed for any significant interaction effects of interest, using Bonferroni corrections for multiple comparisons.

Section 5. Testing for sex differences in effects on LC contrast

To test for sex differences in how HRV biofeedback training affected LC contrast in younger adults, we used a linear mixed effects analysis, specifying fixed effects of training condition, timepoint, hemisphere, sex and their interactions and LC contrast as the dependent variable. To test for sex differences in the association between LC contrast change and training oscillatory power, we performed another analysis, specifying fixed effects of training power, hemisphere, sex, and their interactions and change in LC contrast as the dependent variable. For these analyses, sex was coded as female = 0.5, male = -0.5.

Supplementary Results

Section 1. Analysis of distance between pre- and post-training peak LC locations

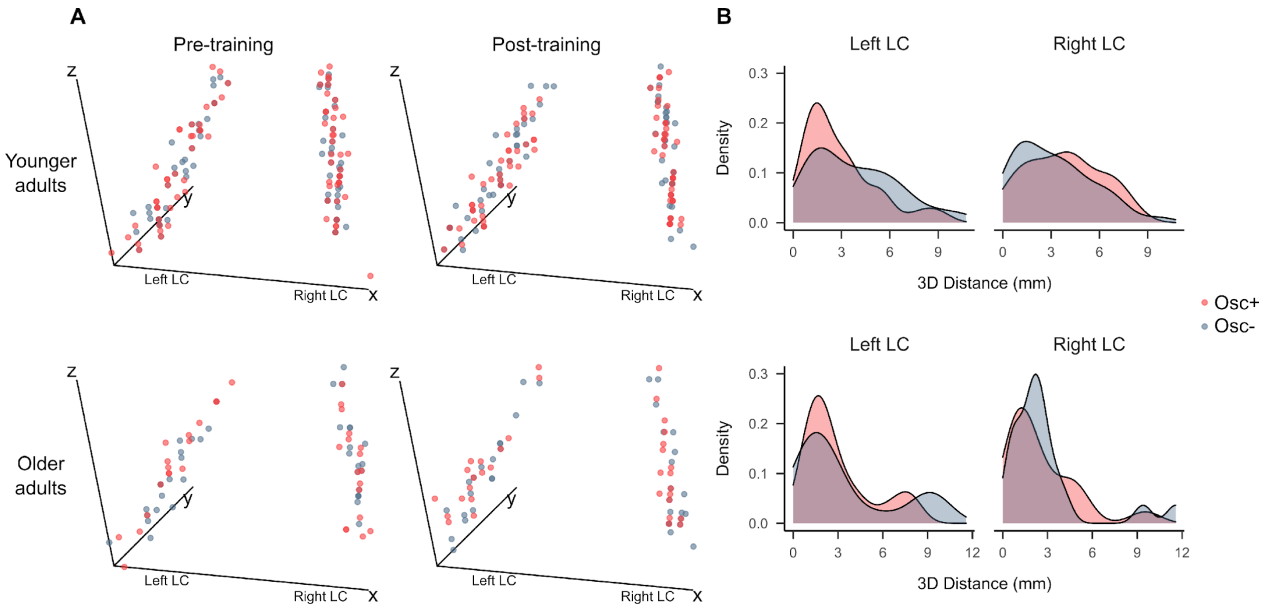

Figure S2. (A) Coordinates of peak LC signal intensity at the pre- and post-training timepoints in MNI152 0.5mm linear standard space. Coordinates range from x = 192 (left) to 168 (right), y = 172 (front) to 182 (back), z = 85 (bottom) to 112 (top). (B) Density plots depicting 3-dimensional distance in millimeters between each participant's peak LC intensity coordinates at the pre- and post-training timepoints. Osc+ = increase-oscillations condition; Osc- = decrease-oscillations condition.

Table S2:

Results of a linear mixed effects analysis testing the fixed effects of training condition, age group and hemisphere on 3-dimensional distance between pre- and post-training peak LC intensity locations.

Predictor	Estimate	SE	95% CI	t	p
Intercept	1.648	0.052	1.545, 1.75	31.513	**<.001**
Condition	-0.050	0.105	-0.255, 0.155	-0.476	0.635
Hemisphere	0.048	0.095	-0.139, 0.235	0.507	0.613
Age group	-0.144	0.105	-0.349, 0.061	-1.380	0.170
Condition x Hemisphere	-0.186	0.191	-0.559, 0.188	-0.975	0.332
Condition x Age group	0.001	0.209	-0.409, 0.411	0.006	0.995
Hemisphere x Age group	0.133	0.191	-0.241, 0.506	0.697	0.488
Condition x Hemisphere x Age group	0.500	0.381	-0.247, 1.247	1.311	0.193

Note. Model included random intercepts for participants. Factors were coded as: condition (Osc+ = 0.5, Osc- = -0.5), age group (older = 0.5, younger = -0.5), hemisphere (left = 0.5, right = -0.5). Distance values were square root transformed prior to analysis as a correction for non-normality, which was indicated by a significant Shapiro-Wilk test ($W = 0.904$, $p < .001$). The significant intercept term indicates that distances differed from 0 across conditions, age groups and hemispheres.

Section 2. Analysis of training effects on LC contrast

Table S3:

Results of a linear mixed effects analysis testing the fixed effects of timepoint, training condition, age group and hemisphere on LC contrast.

Predictor	Estimate	SE	95% CI	t	p
Intercept	0.051	0.004	0.042, 0.059	11.903	**<.001**
Timepoint	0.007	0.004	-0.002, 0.015	1.607	0.109
Condition	0.004	0.009	-0.012, 0.021	0.511	0.611
Hemisphere	0.050	0.004	0.041, 0.058	11.463	**<.001**
Age group	0.031	0.009	0.015, 0.048	3.679	**<.001**
Timepoint x Condition	-0.008	0.009	-0.025, 0.009	-0.895	0.371
Timepoint x Hemisphere	-0.006	0.009	-0.023, 0.011	-0.690	0.491
Condition x Hemisphere	0.012	0.009	-0.005, 0.029	1.338	0.182
Timepoint x Age group	0.015	0.009	-0.002, 0.032	1.736	0.084
Condition x Age group	0.007	0.017	-0.026, 0.04	0.419	0.676
Hemisphere x Age group	-0.008	0.009	-0.025, 0.009	-0.931	0.353
Timepoint x Condition x Hemisphere	-0.005	0.017	-0.039, 0.029	-0.267	0.790
Timepoint x Condition x Age group	0.026	0.017	-0.008, 0.06	1.505	0.133
Timepoint x Hemisphere x Age group	0.017	0.017	-0.017, 0.051	0.971	0.332
Condition x Hemisphere x Age group	0.002	0.017	-0.032, 0.036	0.096	0.924

Predictor	Estimate	SE	95% CI	t	p
Timepoint x Condition x Hemisphere x Age group	0.016	0.035	-0.052, 0.084	0.469	0.639

Note. Model included random intercepts for participants. Factors were coded as: timepoint (post-training = 0.5, pre-training = -0.5), condition (Osc+ = 0.5, Osc- = -0.5), age group (older = 0.5, younger = -0.5), hemisphere (left = 0.5, right = -0.5).

Section 3. Analysis of training effects on caudal and rostral LC contrast

Caudal and rostral LC contrast values at each timepoint are visualized in Figure S3A below. Results of linear mixed effects analyses testing the fixed effects of training condition, timepoint, and age group on caudal and rostral LC contrast are presented in Tables S4 and S5, respectively. For caudal LC contrast, there were no significant training condition x timepoint or training condition x timepoint x age group interaction effects (*p*'s >= .421; Table S4). For rostral LC contrast, there was a significant training condition x timepoint x age group interaction effect (*p* = .044; Table S5) but no significant training condition x timepoint interaction effect (*p* = 0.764; Table S5). This 3-way interaction effect was driven by decreases in rostral LC contrast for younger participants in the Osc+ condition and decreases for younger participants in the Osc- condition, and the opposite pattern in older participants, although no pairwise comparisons of rostral LC contrast were significant (*p*'s >= .213).

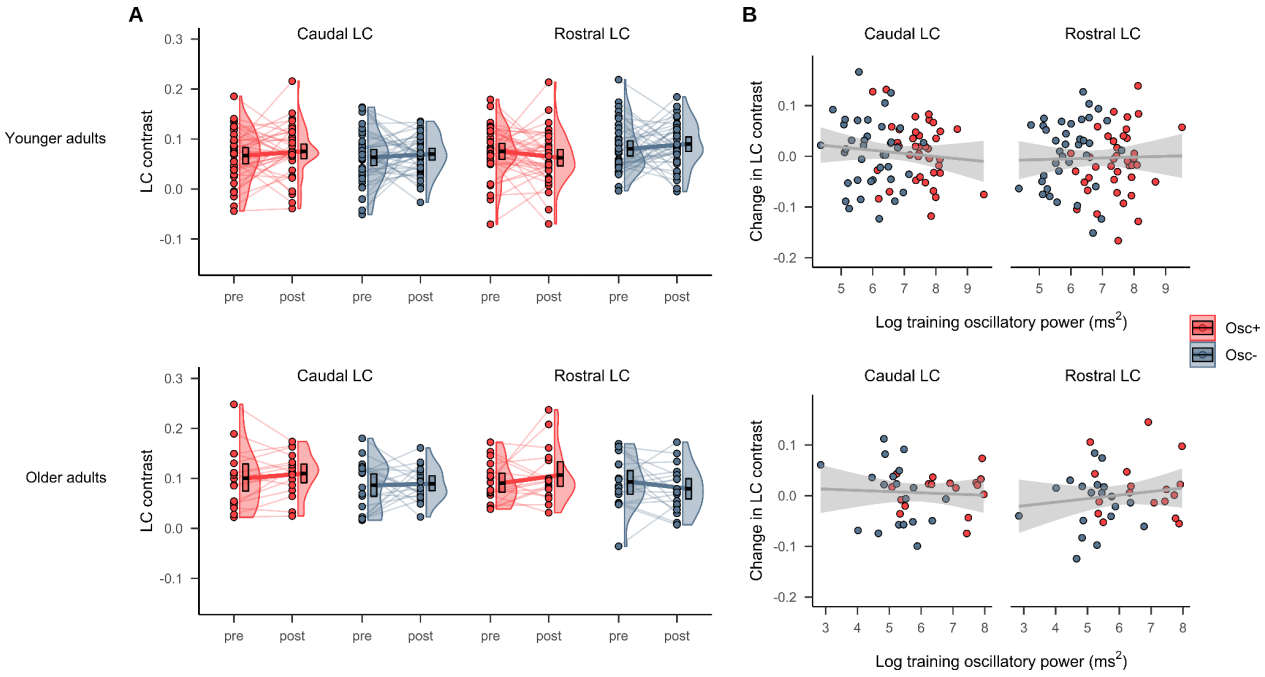

Figure S3. (A) Caudal and rostral LC MRI contrast at the pre- and post-training timepoints for the Osc+ and Osc- conditions, for younger (top) and older (bottom) participants. (B) Associations between pre- to post-training change in caudal and rostral LC contrast and training oscillatory power, a measure of how much participants increased their heart rate oscillations across practice sessions, for younger (top) and older (bottom) participants. Linear regression lines with 95% confidence intervals are shown in gray.

Table S4:

Results of a linear mixed effects analysis testing the fixed effects of timepoint, training condition, and age group on caudal LC contrast.

Predictor	Estimate	SE	95% CI	t	p
Intercept	0.083	0.004	0.075, 0.090	21.043	**<.001**
Timepoint	0.007	0.006	-0.005, 0.018	1.139	.257
Condition	0.011	0.008	-0.004, 0.026	1.388	.168
Age group	0.027	0.008	0.012, 0.043	3.480	**<.001**
Timepoint x Condition	0.004	0.012	-0.019, 0.027	0.342	.733
Timepoint x Age group	-0.001	0.012	-0.024, 0.022	-0.105	.917
Condition x Age group	0.013	0.016	-0.018, 0.044	0.808	.421
Timepoint x Condition x Age group	0.004	0.024	-0.043, 0.050	0.165	.869

Note. Model included random intercepts for participants. Factors were coded as: timepoint (post-training = 0.5, pre-training = -0.5), condition (Osc+ = 0.5, Osc- = -0.5), age group (older = 0.5, younger = -0.5).

Table S5:

Results of a linear mixed effects analysis testing the fixed effects of timepoint, training condition, and age group on rostral LC contrast.

Predictor	Estimate	SE	95% CI	t	p
Intercept	0.085	0.004	0.077, 0.092	22.473	**<.001**
Timepoint	0.000	0.006	-0.013, 0.012	-0.033	.974
Condition	-0.002	0.008	-0.017, 0.013	-0.265	.792
Age group	0.015	0.008	0.001, 0.030	2.035	**.044**
Timepoint x Condition	0.004	0.013	-0.021, 0.029	0.302	.764
Timepoint x Age group	0.003	0.013	-0.022, 0.028	0.221	.826
Condition x Age group	0.029	0.015	-0.001, 0.059	1.927	.057
Timepoint x Condition x Age group	0.052	0.026	0.002, 0.102	2.035	**.044**

Note. Model included random intercepts for participants. Factors were coded as: timepoint (post-training = 0.5, pre-training = -0.5), condition (Osc+ = 0.5, Osc- = -0.5), age group (older = 0.5, younger = -0.5).

Associations between changes in caudal and rostral LC contrast and training oscillatory power are presented in Figure S3B. Training oscillatory power was not significantly correlated with change in caudal LC contrast in either younger ($r(74) = -0.106$, *95% CI* = -0.324 - 0.123, $p = .363$) or older participants ($r(34) = -0.058$, *95% CI* = -0.379 - 0.276, $p = .739$). Training power was also not significantly correlated with change in rostral LC contrast in either younger ($r(74) = -0.026$, *95% CI* = -0.201 - 0.250, $p = .823$) or older participants ($r(34) = 0.150$, *95% CI* = -0.188 - 0.456, $p = .383$).

Section 4. Analysis of associations between training power and change in LC contrast

Table S6:

Results of a linear mixed effects analysis testing fixed effects of training oscillatory power, age group and hemisphere on change in LC contrast.

Predictor	Estimate	SE	95% CI	t	p
Intercept	0.031	0.027	-0.022, 0.083	1.147	0.254
Training power	-0.003	0.004	-0.012, 0.005	-0.823	0.412
Hemisphere	0.029	0.035	-0.04, 0.098	0.830	0.408
Age group	-0.059	0.054	-0.164, 0.046	-1.104	0.272
Training power x Hemisphere	-0.005	0.006	-0.016, 0.006	-0.970	0.334
Training power x Age group	0.011	0.008	-0.005, 0.028	1.351	0.179
Hemisphere x Age group	-0.023	0.071	-0.162, 0.115	-0.332	0.741
Training power x Hemisphere x Age group	0.006	0.011	-0.016, 0.027	0.505	0.614

Note. Model included random intercepts for participants. Factors were coded as: age group (older = 0.5, younger = -0.5), hemisphere (left = 0.5, right = -0.5).

Section 5. Analysis of sex differences in LC contrast change

Table S7:

Results of a linear mixed effects model testing the fixed effects of timepoint, training condition, hemisphere, and sex on LC contrast.

Predictor	Estimate	SE	95% CI	t	p
Intercept	0.034	0.004	0.025, 0.043	7.554	**<.001**
Timepoint	-0.001	0.005	-0.011, 0.008	-0.218	0.828
Condition	-0.003	0.009	-0.021, 0.014	-0.373	0.710
Hemisphere	0.052	0.005	0.042, 0.061	10.714	**<.001**
Sex	0.025	0.009	0.007, 0.042	2.794	**0.007**
Timepoint x Condition	-0.021	0.010	-0.04, -0.002	-2.159	**0.032**
Timepoint x Hemisphere	-0.014	0.010	-0.033, 0.005	-1.463	0.145
Condition x Hemisphere	0.011	0.010	-0.008, 0.03	1.138	0.256
Timepoint x Sex	-0.003	0.010	-0.022, 0.016	-0.306	0.760
Condition x Sex	0.007	0.018	-0.028, 0.042	0.391	0.697
Hemisphere x Sex	-0.017	0.010	-0.036, 0.002	-1.771	0.078
Timepoint x Condition x Hemisphere	-0.012	0.019	-0.05, 0.026	-0.613	0.541
Timepoint x Condition x Sex	0.016	0.019	-0.022, 0.054	0.821	0.412
Timepoint x Hemisphere x Sex	-0.006	0.019	-0.044, 0.032	-0.290	0.772
Condition x Hemisphere x Sex	0.061	0.019	0.023, 0.099	3.165	**0.002**

Predictor	Estimate	SE	95% CI	t	p
Timepoint x Condition x Hemisphere x Sex	0.000	0.039	-0.076, 0.076	0.010	0.992

Note. Model included random intercepts for participants. Factors were coded as: timepoint (post-training = 0.5, pre-training = -0.5), condition (Osc+ = 0.5, Osc- = -0.5), age group (older = 0.5, younger = -0.5), hemisphere (left = 0.5, right = -0.5), sex (female = 0.5, male = -0.5). Only data from younger adults was used for this analysis.

Supplementary References

Dahl, M. J., Mather, M., Düzel, S., Bodammer, N. C., Lindenberger, U., Kühn, S., & Werkle-Bergner, M. (2019). Rostral locus coeruleus integrity is associated with better memory performance in older adults. *Nature Human Behaviour*, *3*(11), 1203–1214. https://doi.org/10.1038/s41562-019-0715-2

Dahl, M. J., Mather, M., Werkle-Bergner, M., Kennedy, B. L., Guzman, S., Hurth, K., Miller, C. A., Qiao, Y., Shi, Y., Chui, H. C., & Ringman, J. M. (2022). Locus coeruleus integrity is related to tau burden and memory loss in autosomal-dominant Alzheimer's disease. *Neurobiology of Aging*, *112*, 39–54. https://doi.org/10.1016/j.neurobiolaging.2021.11.006

Schneider, C. A., Rasband, W. S., & Eliceiri, K. W. (2012). NIH image to ImageJ: 25 years of image analysis. *Nature Methods*, *9*(7), 671–675. http://www.ncbi.nlm.nih.gov/pubmed/22930834